IOP Publishing Phys. Med. Biol. 65 (2020) 015015 (24pp) https://doi.org/10.1088/1361-6560/ab5b73

Physics in Medicine & Biology

IPEM Institute of Physics and Engineering in Medicine

PAPER

Diffusing alpha-emitters radiation therapy: approximate modeling of the macroscopic alpha particle dose of a point source

RECEIVED
1 August 2019

REVISED
3 November 2019

ACCEPTED FOR PUBLICATION
25 November 2019

PUBLISHED
13 January 2020

Lior Arazi

Unit of Nuclear Engineering, Faculty of Engineering Sciences, Ben-Gurion University of the Negav, POB 653 Beer-Sheva 8410501, Israel

E-mail: larazi@bgu.ac.il

Keywords: alpha-particle, radiation therapy, dosimetry

Abstract

Diffusing alpha-emitters radiation therapy ('DaRT') is a new cancer-treatment modality, which enables treating solid tumors by alpha particles. The treatment utilizes implantable seeds embedded with a low activity of radium-224. Each seed continuously emits the short-lived alpha-emitting daughters of radium-224, which spread over several mm around it, creating a 'kill region' of high alpha-particle dose. DaRT is presently tested in clinical trials, starting with locally advanced and recurrent squamous cell carcinoma (SCC) of the skin and head and neck, with promising results with respect to both efficacy and safety. This work aims to provide a simple model which can serve as a zero-order approximation for DaRT dosimetry, allowing for calculating the macroscopic alpha particle dose of a point source, as a basis for more realistic source geometries. The model consists of diffusion equations for radon-220, lead-212 and bismuth-212, with the other short-lived daughters in local secular equilibrium. For simplicity, the medium is assumed to be homogeneous, isotropic and time-independent. Vascular effects are accounted for by effective diffusion and clearance terms. To leading order, the alpha particle dose can be described by simple analytic expressions, which shed light on the underlying physics. The calculations demonstrate that, for a reasonable choice of model parameters, therapeutic alpha-particle dose levels are obtained over a region measuring 4–7 mm in diameter for sources carrying a few μCi of radium-224. The model predictions served as the basis for treatment planning in the SCC clinical trial, where treatments employing DaRT seeds carrying 2 μCi of radium-224 and spaced 5 mm apart resulted in $\sim$80% complete response of the treated tumors with no observed radiation-induced toxicity. The promising results of the SCC clinical trial indicate that in spite of its approximate nature, the simple diffusion-based dosimetry model provides a quantitative starting point for DaRT treatment planning.

1. Introduction

The concept of Diffusing alpha-emitters radiation therapy (DaRT) was first introduced by Arazi *et al* (2007), as a method for treating solid tumors with alpha particles. In DaRT, tumors are treated by the insertion of specially prepared radioactive sources, loaded with low activities of radium-224 (^{224}Ra), which continuously release from their surface its short-lived alpha-emitting daughter atoms. These spread within the tumor by the combined effects of diffusion and convection (vascular and interstitial), delivering a lethal dose over several mm around each source through their alpha decays.

The ^{224}Ra decay chain is shown in figure 1. The source—a small-diameter cylinder carrying a few μCi of ^{224}Ra several nanometers below its surface—is inserted by a fine-gauge needle applicator into the tumor. Once inside the tumor and over a period determined by the ^{224}Ra half-life (3.632 d), the source releases radon-220 (^{220}Rn, 55.6 s half-life), polonium-216 (^{216}Po, 0.145 s half-life), lead-212 (^{212}Pb, 10.64 h half-life) and thallium-208 (^{208}Tl, 3.053 min half-life) atoms, while ^{224}Ra remains fixed on the source surface[1]. ^{220}Rn, a noble gas, diffuses in

[1] All nuclear data, including isotope half-lives, alpha particle energies and branching ratios are taken from Brookhaven National Laboratory's (BNL) National Nuclear Data Center, NuDat 2.7 online database, www.nndc.bnl.gov/nudat2/ Sonzogni (2005).

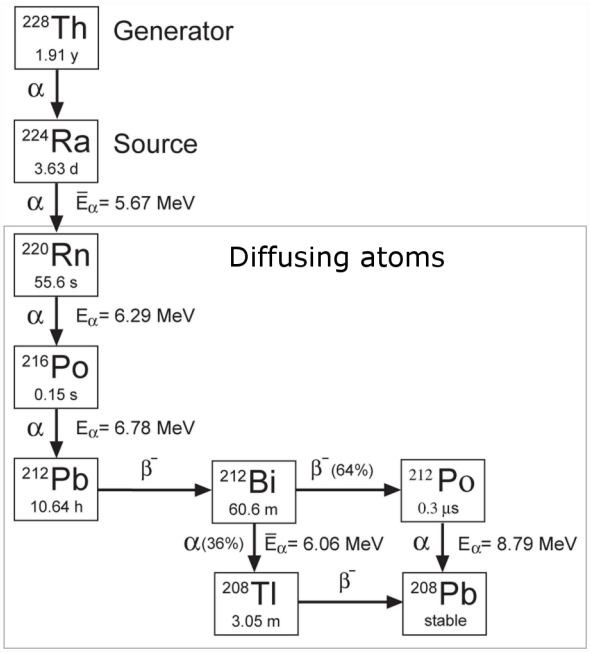

Figure 1. The ^{224}Ra decay chain. Data taken from the NuDat2 database website, www.nndc.bnl.gov/nudat2/

the extra- and intra-cellular space near the source with no chemical interactions, occasionally entering and leaving the porous network of tumoral blood vessels. It contributes two alpha particles through its own decay and through that of its short-lived daughter ^{216}Po, which disintegrates essentially at the same point. ^{212}Pb enters the tumor either by direct release from the source or following the decay of ^{216}Po away from the source, giving rise to a third alpha particle: it beta-decays to bismuth-212 (^{212}Bi, 60.55 min half-life), which either alpha-decays to ^{208}Tl or beta-decays to polonium-212 (^{212}Po, 0.299 μs half-life), which then alpha-decays to stable lead-208. As ^{224}Ra is itself the result of the alpha decay of thorium-228 (^{228}Th, 1.913 y half-life), the production of ^{224}Ra-bearing sources is based on the use of a ^{228}Th generator.

DaRT has been extensively studied *in vitro* and *in vivo* on a large variety of cancer cells and mice-borne tumors of murine and human origin, both as a stand-alone treatment and in conjunction with chemotherapy and immunotherapy (Arazi *et al* 2007, Cooks *et al* 2008, 2009a, 2009b, Lazarov *et al* 2011, Cooks *et al* 2012, Horev-Drori *et al* 2012, Milrot *et al* 2013, Confino *et al* 2015, 2016, Reitkopf-Brodutch *et al* 2015). The insertion of a single DaRT source into tumors with a typical diameter of 5–7 mm was shown to drastically reduce the tumor growth rate for all of the studied cell lines, leading in many cases to significant tumor shrinkage, up to complete regression with no recurrence. Importantly, in all cases of complete regression, there was no sign of damage to the skin adjacent to the tumor.

Autoradiography measurements (Arazi *et al* 2007, Cooks *et al* 2009a, 2012, Horev-Drori *et al* 2012, Reitkopf-Brodutch *et al* 2015) demonstrated that, in all of the tumor models investigated, the alpha emitting atoms indeed spread over significant distances around the source, creating a high-dose 'kill region' measuring several mm in size. In murine squamous cell carcinoma (SCC), for which the largest autoradiography dataset was gathered, the average diameter of the region receiving an estimated alpha particle dose of >10 Gy was ~5–6 mm for sources carrying ~0.4–4 μCi (~15–150 kBq) ^{224}Ra (Arazi *et al* 2007). While a considerable fraction of the ^{212}Pb activity leaves the tumor through the blood and spreads throughout the body, biokinetic and internal-dosimetry modeling of this effect in humans showed that the expected dose to distant organs falls at least an order of magnitude below the maximal tolerated levels for realistic treatment scenarios (Arazi *et al* 2010).

Starting in 2017, DaRT is under investigation in clinical trials, within the framework of Alpha TAU Medical Ltd. The first-in-human study focuses on locally advanced and recurrent SCC of the skin and head and neck, and its initial results are reported on in a recent publication (Popovtzer *et al* 2019). Tumors were treated by the insertion of multiple DaRT sources ('seeds'), each carrying 2 μCi (74 kBq) ^{224}Ra, at a nominal spacing of 5 mm (in more recent treatments the seed activity was changed to 3 μCi). All treated tumors displayed positive response (30%–100% shrinkage) starting within days after the treatment, and close to 80% showed complete regression, with no relapse in the vast majority of cases within the followup period. Side effects in all cases were mild to moderate, with no sign of radiation-induced damage to adjacent tissue or distant organs. Radioactivity measurements of ^{212}Pb in the blood and urine were consistent with the predictions of the biokinetic model (Arazi *et al* 2010), with typical estimated organ doses of a few cGy.

The recent introduction of DaRT in clinical settings calls for the development of detailed tumor dosimetry. This is a broad effort, which will be divided into several publications, with the aim of laying the theoretical basis for DaRT dosimetry, and provide a quantitative starting point for treatment planning. The present manuscript focuses on a zero-order approximate model for the *macroscopic* alpha particle dose, introducing the key parameters influencing the spread of alpha emitters in the treated tumor and understanding the spatial and temporal behavior of the dose profile. We present the basic assumptions leading to the model equations and solve them numerically for the case of an ideal point source, as a basic building block for more complicated geometries. We further describe approximate solutions to the model equations, providing physically-motivated dose estimations without resorting to full numerical computation. The subsequent theoretical publications will extend the discussion to additional source geometries and arrays of multiple sources, provide calculations of the beta and gamma dose, and relate the macroscopic dose estimates to microdosimetric quantities. An additional manuscript will discuss in detail the experimental methodology employed to determine the model parameters.

2. General considerations regarding the transport of ^{224}Ra progeny inside the tumor

The tumor microenvironment into which ^{224}Ra releases its daughters is complex and dynamic. The local properties of the medium can substantially vary between different sub-regions of the tumor, and may also change with time—both because of 'normal' biological processes (e.g. cell division) and due to the treatment itself, which leads to the formation of a necrotic region around the source. The removal of dead cell debris results in tumor shrinkage—starting within the first few days after the treatment (Popovtzer *et al* 2019)—which, in turn, can bring the seeds closer together.

The vascular architecture of the tumor, which affects the migration of ^{224}Ra progeny atoms both through convection and partial clearance, is very different from that of normal tissue (Jain and Baxter 1988). The tumor interior is largely avascular and necrotic (or semi-necrotic), while the outer regions comprise the angiogenically-formed blood network. The tumor vascular system is highly chaotic, consisting of thin and leaky tortuous capillaries, with nearby 'pools' of still fluid. Since tumors do not have a lymphatic network, fluids slowly ooze out by interstitial flow, driven by the elevated interstitial fluid pressure in the tumor bulk (Jain 2001).

^{224}Ra progeny atoms migrate through this complicated heterogeneous environment by a combination of diffusion and convection (vascular and interstitial). Luckily, of the six radionuclides entering the tumor, only three—^{220}Rn, ^{212}Pb and ^{212}Bi – warrant detailed discussion. The other three isotopes—^{216}Po, ^{212}Po and ^{208}Tl—are sufficiently short-lived to safely assume that they are in local secular equilibrium with their parents. In the following section we write the most general equations describing the transport of ^{220}Rn, ^{212}Pb and ^{212}Bi through the tumor, before turning to the simplified approach described in section 3.

2.1. ^{220}Rn and ^{216}Po

^{220}Rn leaves the source surface with a desorption probability $P_{des}(\mathrm{Rn}) \sim 40\%$—i.e. for each decay of ^{224}Ra below the surface there is a $\sim$40% probability that ^{220}Rn will enter the tumor. $P_{des}(\mathrm{Rn})$ is determined experimentally by alpha spectroscopy, as described in appendix A. ^{220}Rn release from the source occurs by direct recoil, with a maximal kinetic energy of 103 keV. The recoiling atom, which most likely enters the tumor as a positive ion (Cano and Dressel 1965, Gunter *et al* 1966) slows down within a few nm to thermal energy, collects its missing electrons and continues by diffusion[2].

The migration of ^{220}Rn inside the tissue can be described in the most general form (in the framework of a continuum approach) by the following transport equation:

$$\frac{\partial n_{\mathrm{Rn}}}{\partial t} + \nabla \cdot \mathbf{j}_{\mathrm{Rn}} = s_{\mathrm{Rn}} - \lambda_{\mathrm{Rn}} n_{\mathrm{Rn}} \tag{1}$$

where $n_{\mathrm{Rn}}(\mathbf{r}, t)$ is the local concentration (number density) of ^{220}Rn atoms (in units of cm^{-3}), $s_{\mathrm{Rn}}(\mathbf{r}, t)$ is the ^{220}Rn source term (in units of cm^{-3} s^{-1}), and λ_{Rn} is the decay rate constant $\left(\lambda = \ln 2/\tau_{1/2}\right)$. The current density $\mathbf{j}_{\mathrm{Rn}}(\mathbf{r}, t)$ is the net vector flux of ^{220}Rn atoms (in units of cm^{-2} s^{-1}). In the most general case, it is composed of both diffusive and convective terms:

$$\mathbf{j}_{\mathrm{Rn}}(\mathbf{r}, t) = -D_{\mathrm{Rn}}(\mathbf{r}, t)\, \nabla n_{\mathrm{Rn}}(\mathbf{r}, t) + n_{\mathrm{Rn}}(\mathbf{r}, t)\, \mathbf{v}(\mathbf{r}, t) \tag{2}$$

where $D_{\mathrm{Rn}}(\mathbf{r}, t)$ is the local effective diffusion coefficient (in units of cm^2 s^{-1}) and $\mathbf{v}(\mathbf{r}, t)$ is the local fluid velocity field (describing both blood and interstitial fluid flow). Note that both the diffusion coefficient and velocity field depend, in general, on space and time. The spatial dependence may be characterized by abrupt changes over cellular distances. The temporal dependence, describing biological processes occurring inside the tissue (in part, as a result of the treatment itself), is characterized by changes occurring over a typical time scale of days.

[2] An alternative source production method involves the application of a thin polymer layer on the source surface. In this case, 220Rn diffuses out from the layer into the tumor as a neutral atom.

In the absence of inadvertent ^{224}Ra release from the DaRT source, $s_{\mathrm{Rn}}(\mathbf{r},t)$ is described mathematically as a delta function for a point source, or as a flux boundary condition for a finite source. For a point source:

$$s_{\mathrm{Rn}}(\mathbf{r},t) = P_{des}(\mathrm{Rn})\Gamma^{src}_{\mathrm{Ra}}(0)\, e^{-\lambda_{\mathrm{Ra}}t}\delta(\mathbf{r}) \tag{3}$$

where $t=0$ is the time of source insertion into the tumor and $\Gamma^{src}_{\mathrm{Ra}}(t) = \Gamma^{src}_{\mathrm{Ra}}(0)\, e^{-\lambda_{\mathrm{Ra}}t}$ is the ^{224}Ra activity on the source.

^{216}Po enters the tumor either by recoil (with a maximal kinetic energy of 116 keV), following alpha decays of ^{220}Rn below the source surface, or by alpha decays of ^{220}Rn away from the source. The diffusive spread of ^{216}Po inside the tissue can be estimated based on its mean lifetime, $\tau_{\mathrm{Po216}} \simeq 0.2$ s, and an order-of-magnitude estimate for its diffusion coefficient $D_{\mathrm{Po216}} \sim 10^{-6}$ cm^{2}s^{-1} (which is typical for positive ions in water):

$$^{216}\mathrm{Po}\ \textit{spread} \sim \sqrt{D_{\mathrm{Po216}}\tau_{\mathrm{Po216}}} \sim 4\ \mu\mathrm{m}. \tag{4}$$

Hence, for all practical purposes, ^{216}Po emitted from the source decays essentially on the source surface, while ^{216}Po created away from the source is in local secular equilibrium with ^{220}Rn and their specific activities are the same:

$$\lambda_{\mathrm{Po216}} n_{\mathrm{Po216}}(\mathbf{r},t) = \lambda_{\mathrm{Rn}} n_{\mathrm{Rn}}(\mathbf{r},t). \tag{5}$$

2.2. ^{212}Pb

The next radionuclide in the chain is ^{212}Pb, which enters the tumor via three possible routes: (1) direct recoil from the source (with a maximal kinetic energy of 128 keV), following ^{216}Po alpha decay events below its surface; (2) alpha decays of ^{216}Po atoms which have recoiled out of the source and (3) alpha decays of ^{216}Po following ^{220}Rn decays away from the source. Summed over these three possible routes, the *effective desorption probability* of ^{212}Pb, $P^{eff}_{des}(\mathrm{Pb})$ (i.e. the total probability that a ^{212}Pb atom enters the tumor following a ^{224}Ra decay event on the source), is found experimentally to be $\sim$55%, employing a methodology described in appendix A.

Following its creation, ^{212}Pb probably remains a free ion for a short while (Lide 2008). It is well known, however, that the percentage of bio-available lead (i.e. free lead ions) in tissue is very low (Payne *et al* 1999). Thus, the free ion state is short-lived and ^{212}Pb can be assumed to rapidly bind to various surrounding proteins (Griffin and Matson 1972, Fowler 1998, Smith *et al* 1998). The ^{212}Pb population inside the tumor is therefore likely composed of several molecular species, each having its own effective diffusion coefficient (depending on the mass and shape of the binding protein), which may also interchange ^{212}Pb among themselves. It is further well established that $\sim$99% of stable lead atoms inside the blood are concentrated inside the red blood cells (RBCs). The typical time it takes a lead atom to pass from the plasma to the RBCs is of the order of a few minutes, while the typical time characterizing the opposite transition (RBCs to plasma) is several days (Leggett 1993). Thus, red blood cells effectively act as traps for ^{212}Pb atoms entering the blood.

This complicated problem may be described by a set of equations, each pertaining to one ^{212}Pb molecular species, with its own diffusion coefficient and source terms, and with additional terms describing ^{212}Pb exchange between species. However, in the absence of detailed information required for such complete analysis, we choose here to lump all species together, leading to

$$\frac{\partial n_{\mathrm{Pb}}}{\partial t} + \nabla\cdot\mathbf{j}_{\mathrm{Pb}} = s_{\mathrm{Pb}} - \lambda_{\mathrm{Pb}} n_{\mathrm{Pb}}. \tag{6}$$

Here, $n_{\mathrm{Pb}}(\mathbf{r},t)$ is the total ^{212}Pb number density (sum over the number densities of all species), $\mathbf{j}_{\mathrm{Pb}}(\mathbf{r},t)$ is the total current density, $s_{\mathrm{Pb}}(\mathbf{r},t)$ is the source term (describing ^{212}Pb creation following ^{216}Po decays on the source and inside the tumor) and λ_{Pb} is the radioactive decay rate constant. Similar to ^{220}Rn, the ^{212}Pb current density comprises diffusive and convective terms:

$$\mathbf{j}_{\mathrm{Pb}}(\mathbf{r},t) = -D_{\mathrm{Pb}}(\mathbf{r},t)\nabla n_{\mathrm{Pb}}(\mathbf{r},t) + n_{\mathrm{Pb}}(\mathbf{r},t)\,\mathbf{v}(\mathbf{r},t) \tag{7}$$

where $D_{\mathrm{Pb}}(\mathbf{r},t)$ is the local effective diffusion coefficient, representing a weighted average over the diffusion coefficients of all species. For the case of a point source, the source term is

$$\begin{aligned} s_{\mathrm{Pb}}(\mathbf{r},t) &= \lambda_{\mathrm{Po216}} n_{\mathrm{Po216}}(\mathbf{r},t) + \left(P^{eff}_{des}(\mathrm{Pb}) - P_{des}(\mathrm{Rn})\right)\Gamma^{src}_{\mathrm{Ra}}(0)\, e^{-\lambda_{\mathrm{Ra}}t}\delta(\mathbf{r}) \\ &= \lambda_{\mathrm{Rn}} n_{\mathrm{Rn}}(\mathbf{r},t) + \left(P^{eff}_{des}(\mathrm{Pb}) - P_{des}(\mathrm{Rn})\right)\Gamma^{src}_{\mathrm{Ra}}(0)\, e^{-\lambda_{\mathrm{Ra}}t}\delta(\mathbf{r}) \end{aligned} \tag{8}$$

where we have assumed local secular equilibrium between ^{216}Po and ^{220}Rn (equation (5)).

2.3. ^{212}Bi, ^{212}Po and ^{208}Tl

Since typical recoil kinetic energies in beta decays are a few eV, ^{212}Bi is generally not emitted directly from the source, but is rather created inside the tumor in ^{212}Pb decays. Similarly to its parent, it might also exist in several

molecular forms. The transport equation relating to the total ^{212}Bi number density can be derived in a similar fashion (by summing over all species):

$$\frac{\partial n_{\mathrm{Bi}}}{\partial t} + \nabla \cdot \mathbf{j}_{\mathrm{Bi}} = s_{\mathrm{Bi}} - \lambda_{\mathrm{Bi}} n_{\mathrm{Bi}}. \tag{9}$$

In this case, the source term is simply

$$s_{\mathrm{Bi}}(\mathbf{r}, t) = \lambda_{\mathrm{Pb}} n_{\mathrm{Pb}}(\mathbf{r}, t) \tag{10}$$

^{212}Po is in local secular equilibrium with ^{212}Bi and hence (figure 1):

$$\lambda_{\mathrm{Po212}} n_{\mathrm{Po212}}(\mathbf{r}, t) = 0.64\, \lambda_{\mathrm{Bi}} n_{\mathrm{Bi}}(\mathbf{r}, t). \tag{11}$$

Although ^{208}Tl, with its 3 min half-life, may show some redistribution relative to ^{212}Bi, this effect is of little dosimetric importance. Hence we assume that, like ^{212}Po, ^{208}Tl is in secular equilibrium with ^{212}Bi:

$$\lambda_{\mathrm{Tl}} n_{\mathrm{Tl}}(\mathbf{r}, t) = 0.36\, \lambda_{\mathrm{Bi}} n_{\mathrm{Bi}}(\mathbf{r}, t). \tag{12}$$

3. The diffusion-leakage model

The full-blown transport equations given above provide the most general framework for describing the migration of ^{224}Ra progeny atoms inside the tissue. However, they are of limited practical use, since their complete solution requires detailed three-dimensional and time-dependent information on the sub-mm scale which is presently unavailable in clinical settings. It is thus natural to seek approximate modeling techniques that, while avoiding any pretension to accurately describe this highly complicated problem, will provide quantitative dosimetric estimates that could serve as a starting point for actual treatment planning. We propose a simple model to that effect, based on the following simplifying assumptions.

- ^{224}Ra daughter migration inside the tumor is predominantly diffusive. Vascular convection by the tortuous capillaries is characterized by a short correlation length (relative to therapeutically significant distances) and can thus be incorporated into an effective diffusion coefficient. Interstitial convection is neglected.
- The tissue is homogeneous, isotropic and time-independent. All model parameters are constant in space and time.
- ^{212}Pb migration can be described using a single effective diffusion coefficient representing the average over all ^{212}Pb molecular species.
- ^{212}Pb atoms reaching major blood vessels are trapped in red blood cells and immediately cleared from the tumor. This process is described by a uniform volumetric sink term. The finite clearance rate reflects the time it takes migrating ^{212}Pb atoms to reach such traps.
- Since the short-lived ^{220}Rn atoms are free to diffuse with no chemical interaction through blood vessels and RBCs, the equation for ^{220}Rn does not include a sink term (i.e. blood vessels do not act as traps for ^{220}Rn).
- The diffusion equation for ^{212}Bi does include a sink term. However, this is considered a second order effect.

Under these assumptions, the number densities of ^{220}Rn, ^{212}Pb and ^{212}Bi are governed by the following diffusion equations:

$$\frac{\partial n_{\mathrm{Rn}}}{\partial t} = D_{\mathrm{Rn}} \nabla^2 n_{\mathrm{Rn}} + s_{\mathrm{Rn}} - \lambda_{\mathrm{Rn}} n_{\mathrm{Rn}} \tag{13}$$

$$\frac{\partial n_{\mathrm{Pb}}}{\partial t} = D_{\mathrm{Pb}} \nabla^2 n_{\mathrm{Pb}} + s_{\mathrm{Pb}} - \lambda_{\mathrm{Pb}} n_{\mathrm{Pb}} - \alpha_{\mathrm{Pb}} n_{\mathrm{Pb}} \tag{14}$$

$$\frac{\partial n_{\mathrm{Bi}}}{\partial t} = D_{\mathrm{Bi}} \nabla^2 n_{\mathrm{Bi}} + \lambda_{\mathrm{Pb}} n_{\mathrm{Pb}} - \lambda_{\mathrm{Bi}} n_{\mathrm{Bi}} - \alpha_{\mathrm{Bi}} n_{\mathrm{Bi}}. \tag{15}$$

Note that the clearance (sink) term in equation (14) is given by $\alpha_{\mathrm{Pb}} n_{\mathrm{Pb}}$, where $1/\alpha_{\mathrm{Pb}}$ is the average clearance time. The corresponding term in equation (15) is $\alpha_{\mathrm{Bi}} n_{\mathrm{Bi}}$.

4. Integral properties of the diffusion-leakage model

Before delving into the spatial and temporal properties of the solutions to equations (13)–(15), it is worthwhile to investigate the integral properties of these equations. This provides insights on quantities which can be determined experimentally, and helps bracketing the values of some of the model parameters. We begin by rewriting equations (13)–(15) in a form that gives explicit representation of the current terms:

$$\frac{\partial n_{\mathrm{Rn}}}{\partial t} + \nabla \cdot \mathbf{j}_{\mathrm{Rn}} = s_{\mathrm{Rn}} - \lambda_{\mathrm{Rn}} n_{\mathrm{Rn}} \tag{16}$$

$$\frac{\partial n_{\mathrm{Pb}}}{\partial t} + \nabla \cdot \mathbf{j}_{\mathrm{Pb}} = s_{\mathrm{Pb}} - \left(\lambda_{\mathrm{Pb}} + \alpha_{\mathrm{Pb}}\right) n_{\mathrm{Pb}} \tag{17}$$

$$\frac{\partial n_{\mathrm{Bi}}}{\partial t} + \nabla \cdot \mathbf{j}_{\mathrm{Bi}} = \lambda_{\mathrm{Pb}} n_{\mathrm{Pb}} - \left(\lambda_{\mathrm{Bi}} + \alpha_{\mathrm{Bi}}\right) n_{\mathrm{Bi}}. \tag{18}$$

We now integrate the equations over all space. We assume that the tumor is large enough so that the current densities vanish on its external boundary (this assumption holds to an accuracy of $<1\%$ if the tumor radius is of the order of a few mm as discussed below). We reiterate that ^{212}Pb and ^{212}Bi leakage from the tumor is considered, in this model, to be a volumetric effect (described by the respective sink terms $\alpha_{\mathrm{Pb}} n_{\mathrm{Pb}}$ and $\alpha_{\mathrm{Bi}} n_{\mathrm{Bi}}$), rather than a surface effect. Thus, the current densities can be assumed to vanish on the periphery without contradicting the observed leakage of radionuclides from the tumor through the blood.

The total number of atoms of species k inside the tumor, $N_k^{tum}(t)$, is

$$N_k^{tum}(t) = \int_{\Omega} n_k(\mathbf{r}, t)\, d^3\mathbf{r} \tag{19}$$

where Ω denotes the entire tumor. The volume integral of the current terms (for all species) is evaluated using the divergence theorem:

$$\int_{\Omega} \nabla \cdot \mathbf{j}_k d^3\mathbf{r} = \int_{\partial\Omega} \mathbf{j}_k \cdot \mathbf{n}\, ds = 0 \tag{20}$$

where $\partial\Omega$ denotes the external surface of the tumor and $\mathbf{n}$ is a unit surface vector.

4.1. ^{220}*Rn*

The integrated source term for ^{220}Rn is the rate of ^{220}Rn release from the source:

$$\int_{\Omega} s_{\mathrm{Rn}}\, d^3\mathbf{r} = P_{des}(\mathrm{Rn})\Gamma_{\mathrm{Ra}}^{src}(0)e^{-\lambda_{\mathrm{Ra}}t}. \tag{21}$$

Thus the integral of equation (16) over all space gives

$$\frac{dN_{\mathrm{Rn}}^{tum}}{dt} = P_{des}(\mathrm{Rn})\Gamma_{\mathrm{Ra}}^{src}(0)e^{-\lambda_{\mathrm{Ra}}t} - \lambda_{\mathrm{Rn}} N_{\mathrm{Rn}}^{tum}. \tag{22}$$

Since $N_{\mathrm{Rn}}^{tum}(0) = 0$,the total ^{220}Rn tumor activity $\Gamma_{\mathrm{Rn}}^{tum}(t) = \lambda_{\mathrm{Rn}} N_{\mathrm{Rn}}^{tum}(t)$ is

$$\Gamma_{\mathrm{Rn}}^{tum}(t) = \frac{\lambda_{\mathrm{Rn}}}{\lambda_{\mathrm{Rn}} - \lambda_{\mathrm{Ra}}} P_{des}(\mathrm{Rn})\Gamma_{\mathrm{Ra}}^{src}(0)\left(e^{-\lambda_{\mathrm{Ra}}t} - e^{-\lambda_{\mathrm{Rn}}t}\right). \tag{23}$$

Since $\frac{\lambda_{\mathrm{Rn}}}{\lambda_{\mathrm{Rn}} - \lambda_{\mathrm{Ra}}} = 1.0002$, it converges within several minutes to

$$\Gamma_{\mathrm{Rn}}^{tum}(t) \approx P_{des}(\mathrm{Rn})\Gamma_{\mathrm{Ra}}^{src}(0)e^{-\lambda_{\mathrm{Ra}}t}. \tag{24}$$

4.2. ^{212}Pb

The source term for ^{212}Pb for the case of a point source is given in equation (8). Its integral of over all space gives

$$\begin{aligned}\int_{\Omega} s_{\mathrm{Pb}}(\mathbf{r}, t)\, d^3\mathbf{r} &= \Gamma_{\mathrm{Rn}}^{tum}(t) + \left(P_{des}^{eff}(\mathrm{Pb}) - P_{des}(\mathrm{Rn})\right)\Gamma_{\mathrm{Ra}}^{src}(0)e^{-\lambda_{\mathrm{Ra}}t} \\ &= P_{des}^{eff}(\mathrm{Pb})\Gamma_{\mathrm{Ra}}^{src}(0)e^{-\lambda_{\mathrm{Ra}}t}\end{aligned} \tag{25}$$

where we used equation (24). Thus, the integral of equation (17) over all space gives

$$\frac{dN_{\mathrm{Pb}}^{tum}}{dt} = P_{des}^{eff}(\mathrm{Pb})\Gamma_{\mathrm{Ra}}^{src}(0)e^{-\lambda_{\mathrm{Ra}}t} - \left(\lambda_{\mathrm{Pb}} + \alpha_{\mathrm{Pb}}\right) N_{\mathrm{Pb}}^{tum}. \tag{26}$$

Since $N_{\mathrm{Pb}}^{tum}(0) = 0$ the total tumor ^{212}Pb activity $\Gamma_{\mathrm{Pb}}^{tum}(t) = \lambda_{\mathrm{Pb}} N_{\mathrm{Pb}}^{tum}(t)$ is

$$\Gamma_{\mathrm{Pb}}^{tum}(t) = \frac{\lambda_{\mathrm{Pb}}}{\lambda_{\mathrm{Pb}} + \alpha_{\mathrm{Pb}} - \lambda_{\mathrm{Ra}}} P_{des}^{eff}(\mathrm{Pb})\Gamma_{\mathrm{Ra}}^{src}(0)\left(e^{-\lambda_{\mathrm{Ra}}t} - e^{-(\lambda_{\mathrm{Pb}} + \alpha_{\mathrm{Pb}})t}\right). \tag{27}$$

The initial buildup is characterized by an *effective ^{212}Pb lifetime*, which reflects both its radioactive decay and clearance from the tumor:

$$\tau_{\mathrm{Pb}}^{eff} = \frac{1}{\lambda_{\mathrm{Pb}} + \alpha_{\mathrm{Pb}}}. \tag{28}$$

Depending on the leakage rate coefficient, the total tumor ^{212}Pb activity reaches a maximum ~1–2 days after the treatment.

The total number of ^{212}Pb decays inside the tumor, $N_{decays}^{tum}(\mathrm{Pb})$ is found by integrating $\Gamma_{\mathrm{Pb}}^{tum}(t)$ from zero to infinity:

$$N_{decays}^{tum}(\mathrm{Pb}) = \int_0^\infty \Gamma_{\mathrm{Pb}}^{tum}(t)dt = \frac{\lambda_{\mathrm{Pb}}}{\lambda_{\mathrm{Pb}} + \alpha_{\mathrm{Pb}}} P_{des}^{eff}(\mathrm{Pb}) N_{\mathrm{Ra}}^{src}(0) \tag{29}$$

where $N_{\mathrm{Ra}}^{src}(0) = \Gamma_{\mathrm{Ra}}^{src}(0)\tau_{\mathrm{Ra}}$ is the initial number of ^{224}Ra atoms on the source (for example, for a 3 μCi source $N_{\mathrm{Ra}}^{src}(0) = 5.0 \cdot 10^{10}$). The total number of ^{212}Pb atoms released from the source is

$$N_{rel}(\mathrm{Pb}) = P_{des}^{eff}(\mathrm{Pb}) N_{\mathrm{Ra}}^{src}(0). \tag{30}$$

We define the *^{212}Pb leakage probability* as the probability that a ^{212}Pb atom released from the source decays outside of the tumor. It is equal to one minus the probability that a ^{212}Pb atom released from the source decays inside the tumor. Hence

$$P_{leak}(\mathrm{Pb}) = 1 - \frac{N_{decays}^{tum}(\mathrm{Pb})}{N_{rel}(\mathrm{Pb})} = \frac{\alpha_{\mathrm{Pb}}}{\lambda_{\mathrm{Pb}} + \alpha_{\mathrm{Pb}}}. \tag{31}$$

Depending on the ratio $\alpha_{\mathrm{Pb}}/\lambda_{\mathrm{Pb}}$, $P_{leak}(\mathrm{Pb})$ changes from 0 to 1. In particular, if $\alpha_{\mathrm{Pb}} = \lambda_{\mathrm{Pb}}$, $P_{leak}(\mathrm{Pb}) = \frac{1}{2}$.

4.3. ^{212}Bi

Integrating equation (18) over the entire tumor leads to

$$\frac{dN_{\mathrm{Bi}}^{tum}}{dt} = \lambda_{\mathrm{Pb}} N_{\mathrm{Pb}}^{tum} - (\lambda_{\mathrm{Bi}} + \alpha_{\mathrm{Bi}}) N_{\mathrm{Bi}}^{tum}. \tag{32}$$

The full solution of this equation shows that the total activity of ^{212}Bi follows closely that of ^{212}Pb, lagging by ~2–3 h. For $t \gg \tau_{\mathrm{Pb}}^{eff}$, the asymptotic ratio between the ^{212}Bi and ^{212}Pb activities becomes

$$\frac{\Gamma_{Bi\ asy}^{tum}(t)}{\Gamma_{Pb\ asy}^{tum}(t)} = \frac{\lambda_{\mathrm{Bi}}}{\lambda_{\mathrm{Bi}} + \alpha_{\mathrm{Bi}} - \lambda_{\mathrm{Ra}}}. \tag{33}$$

In the special case $\alpha_{\mathrm{Bi}} = 0$, this ratio equals 1.012. Experimental data in mice SCC tumors (Arazi *et al* 2007) suggest that this is very nearly the case in reality: values measured for tumor samples with masses in the range 20–50 mg were 1.03 ± 0.15, and for 100–200 mg samples—0.98 ± 0.08. Thus, it appears that $\alpha_{\mathrm{Bi}} \ll \lambda_{\mathrm{Bi}}$ and may be set, in most cases, to zero. In other words, ^{212}Bi leaves the tumor primarily as a result of ^{212}Pb clearance by the blood, with no 'independent' leakage.

Figure 2 shows the total (normalized) activity of ^{224}Ra on the source, and the tumor activities of ^{220}Rn, ^{212}Pb and ^{212}Bi, for a typical choice of the desorption probabilities and leakage rate coefficients.

5. Numerical values for the diffusion-leakage model parameters

The predictions of the diffusion-leakage model obviously depend on the choice of numerical values for its parameters—the effective diffusion and leakage rate coefficients. In particular, these parameters, which can vary between tumors of different histologies, determine the size of the 'kill region' of a single DaRT source and the inter-source spacing in DaRT-source lattices. The following section provides reasonable ranges for the values of the model parameters. We rely on both experimental data obtained in mice-borne tumors (for which an example is given in section 7.5, deferring detailed description to a separate publication), and additional information from the literature. We highlight, in particular, the numerical values obtained from experiments on squamous cell carcinoma (SCC) tumors in mice. These presently serve as the starting point for DaRT treatment planning for oral cavity and skin SCC tumors in clinical trials.

5.1. ^{220}*Rn*

Direct measurement of ^{220}Rn diffusion in DaRT-treated mice tumors is challenging because of its one-minute half-life. Our estimates for ^{220}Rn therefore rely on data from the literature.

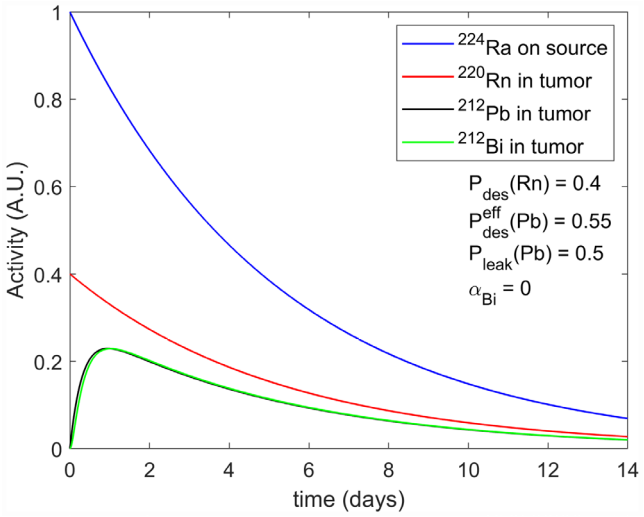

Figure 2. ^{224}Ra activity on the source, and ^{220}Rn, ^{212}Pb and ^{212}Bi activities inside the tumor. The initial conditions are $\Gamma^{src}_{Ra}(0) = 1$ (arbitrary units), $\Gamma^{tum}_{Rn}(0) = \Gamma^{tum}_{Pb}(0) = \Gamma^{tum}_{Bi}(0) = 0$ (the initial buildup of ^{220}Rn is on the scale of minutes and not shown). The ^{212}Pb leakage probability is assumed to be 50% and $\alpha_{Bi} = 0$.

- The diffusion coefficient of radon in water at 37 °C is $1.9 \cdot 10^{-5}$ cm^2 s^{-1} (Jähne *et al* 1987).
- In the NRC report on radon in drinking water (NRC 1999), the authors assumed a value of $0.5 \cdot 10^{-5}$ cm^2 s^{-1} for the diffusion coefficient of radon through the stomach wall, adopting the measured value for xenon as a reference, since no data were available on radon. For comparison, the diffusion coefficient of xenon in water at 35 °C is $1.95 \cdot 10^{-5}$ cm^2 s^{-1} (Lide 2008), similar to that of radon.

Vascular convection may enhance the spread of ^{220}Rn in the blood-rich peripheral regions of the tumor, but is expected to be much less important in the tumor interior. Interstitial flow should have a negligible effect on the spread of ^{220}Rn because of its short half-life and the low flow velocities (~0.1–0.2 μm s^{-1} in animal models and likely ten-fold lower in more realistic scenarios (Jain 2001)).

To conclude, in the tumor interior, the effective diffusion coefficient of ^{220}Rn will be assumed to lie in the range $0.5–2 \cdot 10^{-5}$ cm^2 s^{-1}. The lower bound relies on the NRC report on radon in drinking water. This represents a conservative limit, since tumor tissue may be less fibrous than the stomach wall and will thus hinder ^{220}Rn diffusion to a lesser extent (especially when considering that the tumor tissue is at least partially necrotic). The upper limit allows for possible convective effects to enhance the diffusion coefficient towards its value in water. A representative nominal value would be $1 \cdot 10^{-5}$ cm^2 s^{-1}.

5.2. ^{212}*Pb*

Unlike ^{220}Rn, ^{212}Pb has a sufficiently long half-life to allow for direct measurement of its spread in dissected DaRT-treated mice tumors, as well as of the associated leakage probability. Such measurements therefore supplement expectations based on the available literature.

- As shown in Arazi *et al* (2007), in experimental tumors in mice the ^{212}Pb leakage probability varies in the range ~0.1–0.9, with the majority of cases lying between 0.3 and 0.7, depending on the tumor size[3]. This indicates that the leakage rate coefficient α_{Pb} is of the same order of magnitude as the decay constant λ_{Pb}.
- Using the diffusion-leakage model to analyze autoradiography measurements in mice-borne tumors (Arazi *et al* 2007, Cooks *et al* 2009a, 2012, Horev-Drori *et al* 2012, Reitkopf-Brodutch *et al* 2015), indicates that the effective ^{212}Pb diffusion coefficient lies in the range $\sim 0.2–4 \cdot 10^{-7}$ cm^2 s^{-1}. An example for SCC tumors is given in section 7.5.
- As mentioned above, ^{212}Pb is likely bound to various proteins inside the tumor, with only a small (negligible?) fraction in free ion form Godwin (2001), Payne *et al* (1999). The masses of such proteins (studied in the context of lead toxicity) range from a few kDa (Smith *et al* 1998), through several dozen kDa (Griffin and Matson 1972, Fowler and DuVal 1991, Smith *et al* 1998), up to 280 kDa (Payne *et al* 1999, Godwin 2001). A rough estimate of the possible range of diffusion coefficient values can be made based on data regarding the diffusion coefficient of dextrans (20–150 kDa) in VX2 carcinoma (Jain 1987), which can be approximated by the formula $D = aM^{-b}$, with $a = 2.5 \cdot 10^{-2}$ cm^2 s^{-1} and $b = 1.14$ (M is the molecular

[3] The data shown in Arazi *et al* (2007) concern the fraction of ^{212}Pb activity remaining inside the tumor, which is simply related to P_{leak}(Pb).

mass of the protein). This represents a monotonically decreasing curve, ranging from $3.1 \cdot 10^{-7}$ cm^2 s^{-1} for $M = 20$ kDa down to $3.2 \cdot 10^{-8}$ cm^2 s^{-1} for $M = 150$ kDa. Thus, the empirically estimated range of values for the effective ^{212}Pb diffusion coefficient in murine tumors ($\sim$0.2–$4 \cdot 10^{-7}$ cm^2 s^{-1}) is consistent with a spectrum of protein masses in the range of a few dozen kDa.

Similar to ^{220}Rn, convective flows may have a considerable influence on the spread of ^{212}Pb in the peripheral regions of the tumor. In this case, however, rapid ^{212}Pb clearance following trapping in RBCs is expected to act in the opposite direction and somewhat compensate for this effect. Unlike ^{220}Rn, the long effective lifetime of ^{212}Pb can allow also for a significant contribution by interstitial flows, pushing protein-bound ^{212}Pb atoms radially from the tumor interior towards its periphery, to a degree which may be comparable to the pure-diffusion case.

In summary, based on our preclinical observations, the ^{212}Pb leakage rate coefficient will be assumed to lie in the range $\sim(0.5\text{–}2)\,\lambda_{\mathrm{Pb}}$, i.e. $P_{leak}(\mathrm{Pb}) \sim 0.3\text{–}0.7$, with a nominal value of 0.5. The effective ^{212}Pb diffusion coefficient may be tumor-dependent (and may also depend on the viability of the tissue). It will be assumed to lie in the range $\sim$0.2–$4 \cdot 10^{-7}$ cm^2 s^{-1}. Within the simplistic analysis of the diffusion leakage model, we will presently not describe interstitial and vascular effects.

5.3. ^{212}Bi

Measurements performed on murine SCC tumors suggest that ^{212}Bi and ^{212}Pb are very close to secular equilibrium (driven by ^{224}Ra) throughout the tumor (Arazi *et al* 2007). As noted in section 4, this suggests that $\alpha_{\mathrm{Bi}} \ll \lambda_{\mathrm{Bi}}$. As discussed in appendix B, it also suggests that the effective diffusion coefficient of ^{212}Bi (which may also be bound to various proteins) is considerably smaller than that of ^{212}Pb. In what follows, we will therefore assume that $\alpha_{\mathrm{Bi}} = 0$. As a conservative assumption (in terms of the estimated alpha particle dose) the effective diffusion coefficient of ^{212}Bi will be taken in the range $\sim(0.1\text{–}0.3)D_{\mathrm{Pb}}$.

6. Solving the diffusion-leakage equations for the point source

This section is dedicated to solving the diffusion-leakage equations for the ideal point source. We begin by studying the asymptotic behavior of the solutions for ^{220}Rn, ^{212}Pb and ^{212}Bi, i.e. for times where their respective populations are driven by the exponential decay of ^{224}Ra. The full derivation is given in appendix B while the main results are provided in the text. We then turn our attention to the complete time-dependent solutions. For ^{220}Rn, this is done analytically (with the full derivation given in appendix C). For ^{212}Pb and ^{212}Bi the time dependent equations are solved numerically.

6.1. Asymptotic solutions

The asymptotic forms of the solutions for the diffusion-leakage equations are

$$n_{\mathrm{Rn}}^{asy}(\mathbf{r},t) = \widetilde{n}_{\mathrm{Rn}}(\mathbf{r})\, e^{-\lambda_{\mathrm{Ra}} t} \tag{34}$$

$$n_{\mathrm{Pb}}^{asy}(\mathbf{r},t) = \widetilde{n}_{\mathrm{Pb}}(\mathbf{r})\, e^{-\lambda_{\mathrm{Ra}} t} \tag{35}$$

$$n_{\mathrm{Bi}}^{asy}(\mathbf{r},t) = \widetilde{n}_{\mathrm{Bi}}(\mathbf{r})\, e^{-\lambda_{\mathrm{Ra}} t}. \tag{36}$$

Based on the preceding analysis of the temporal properties of the ^{224}Ra decay chain, this is expected to hold for ^{220}Rn within minutes after source insertion, and for ^{212}Pb and ^{212}Bi within several effective ^{212}Pb lifetimes. As shown below, the time for convergence to the asymptotic form increases with the distance from the source.

6.1.1. ^{220}Rn

As shown in appendix B, inserting (34) into the ^{220}Rn diffusion equation (13) for the point source given in equation (3), leads to

$$n_{\mathrm{Rn}}^{asy}(r,t) = \frac{P_{des}(\mathrm{Rn})\Gamma_{\mathrm{Ra}}^{src}(0)}{4\pi D_{\mathrm{Rn}}} \frac{e^{-r/L_{\mathrm{Rn}}}}{r} e^{-\lambda_{\mathrm{Ra}} t} \tag{37}$$

where we define the *effective ^{220}Rn diffusion length*:

$$L_{\mathrm{Rn}} = \sqrt{\frac{D_{\mathrm{Rn}}}{\lambda_{\mathrm{Rn}} - \lambda_{\mathrm{Ra}}}}. \tag{38}$$

The effective diffusion length is the key parameter which dictates the spatial distribution of the diffusing atoms, and therefore that of the macroscopic alpha particle dose. When the radial distance from the source is increased by one effective diffusion length, the alpha dose drops by $1/e$ (with further reduction arising from the

$1/r$ factor). This spatial dependence is far steeper than the gross $1/r^2$ behavior of (point-like) photon brachytherapy sources, resulting in a much more confined dose field.

The appearance of λ_{Ra} in the definition of the effective diffusion length reflects the fact that the ^{220}Rn population is driven by the exponential decay of ^{224}Ra. Since $\lambda_{Rn} \gg \lambda_{Ra}$, L_{Rn} is very nearly equal to $\sqrt{D_{Rn}\tau_{Rn}}$ (which would be a natural definition for the 'proper' diffusion length; in what follows we will use the terms 'diffusion length' and 'effective diffusion length' interchangeably). For ^{220}Rn diffusion in water ($D_{Rn} = 1.9 \cdot 10^{-5}$cm^2 s^{-1}), $L_{Rn} = 0.39$ mm. For the lower value of the chosen range ($D_{Rn} = 0.5 \cdot 10^{-5}$cm^2 s^{-1}), $L_{Rn} = 0.20$ mm.

The ratio between the outgoing diffusion flux of ^{220}Rn on the surface of a sphere of radius r to its release rate from a source at its center is

$$\frac{4\pi r^2 j_{Rn}(r,t)}{P_{des}(\mathrm{Rn})\Gamma^{src}_{Ra}(t)} = e^{-r/L_{Rn}}\left(1+\frac{r}{L_{Rn}}\right) \tag{39}$$

falling below 1% at $r = 6.6L_{Rn}$. For $L_{Rn} = 0.3$ mm the outgoing diffusion flux is therefore negligible for a tumor radius of $\gtrsim 2$ mm.

6.1.2. ^{212}Pb

For ^{212}Pb we need to consider the source term (8), comprising contributions from the DaRT source and its immediate vicinity and a volumetric term describing ^{220}Rn decays. As discussed in appendix B, substituting the asymptotic forms (34) and (35) in equation (14), yields for $t \gg \tau^{eff}_{Pb}$ for a point ^{224}Ra source:

$$n^{asy}_{Pb}(r,t) = \left(A_{Pb}\frac{e^{-r/L_{Rn}}}{r} + B_{Pb}\frac{e^{-r/L_{Pb}}}{r}\right)e^{-\lambda_{Ra}t} \tag{40}$$

where we define the *effective ^{212}Pb diffusion length*:

$$L_{Pb} = \sqrt{\frac{D_{Pb}}{\lambda_{Pb}+\alpha_{Pb}-\lambda_{Ra}}}. \tag{41}$$

In this case the effective diffusion length comprises the ^{224}Ra mean lifetime, $\tau_{Ra} = 1/\lambda_{Ra}$ and the effective ^{212}Pb lifetime, $\tau^{eff}_{Pb} = \frac{1}{\lambda_{Pb}+\alpha_{Pb}}$, that takes into account the two processes which remove ^{212}Pb atoms from the system—radioactive decay and clearance by the blood. Increased ^{212}Pb removal by the blood thus reduces L_{Pb} leading to a more rapid fall-off of the dose.

As outlined in section 7.5, when analyzed using the diffusion-leakage model, the experimental data from murine SCC tumors (Arazi *et al* 2007) indicate that for this type of tumors L_{Pb} generally lies in the range ~0.5–0.8 mm, while α_{Pb} typically ranges from $0.5\lambda_{Pb}$ to $2\lambda_{Pb}$ (giving $D_{Pb} = 0.6$–$3.3 \cdot 10^{-7}$ cm^2 s^{-1}). Preliminary data from other tumor histologies indicate L_{Pb} values in the range 0.3–0.5 mm (Cooks *et al* 2009a, 2012, Horev-Drori *et al* 2012, Reitkopf-Brodutch *et al* 2015).

The coefficients A_{Pb} and B_{Pb} are given by:

$$A_{Pb} = \left(\frac{L^2_{Rn}L^2_{Pb}}{L^2_{Rn}-L^2_{Pb}}\right)\frac{\lambda_{Rn}}{D_{Pb}}\frac{P_{des}(\mathrm{Rn})\Gamma^{src}_{Ra}(0)}{4\pi D_{Rn}} \tag{42}$$

$$B_{Pb} = \frac{\left(P^{eff}_{des}(\mathrm{Pb}) - P_{des}(\mathrm{Rn})\right)\Gamma^{src}_{Ra}(0)}{4\pi D_{Pb}} - A_{Pb}. \tag{43}$$

Similar to equation (39), the ratio between the outgoing diffusion flux of ^{212}Pb to its release rate from the source falls below 1% for a tumor whose radius is ~2.5–4.5 mm, depending on the assumed values of L_{Rn} and L_{Pb}, justifying the assumption that ^{212}Pb leakage from the tumor is predominantly a volumetric effect.

6.1.3. ^{212}Bi

The procedure for finding the asymptotic solution for ^{212}Bi follows closely the ones for ^{220}Rn and ^{212}Pb and is also described in appendix B. Its general form is given by

$$n^{asy}_{Bi}(r,t) = \left(A_{Bi}\frac{e^{-r/L_{Rn}}}{r} + B_{Bi}\frac{e^{-r/L_{Pb}}}{r} + C_{Bi}\frac{e^{-r/L_{Bi}}}{r}\right)e^{-\lambda_{Ra}t} \tag{44}$$

where we define the *effective ^{212}Bi diffusion length*:

$$L_{Bi} = \sqrt{\frac{D_{Bi}}{\lambda_{Bi}+\alpha_{Bi}-\lambda_{Ra}}} \tag{45}$$

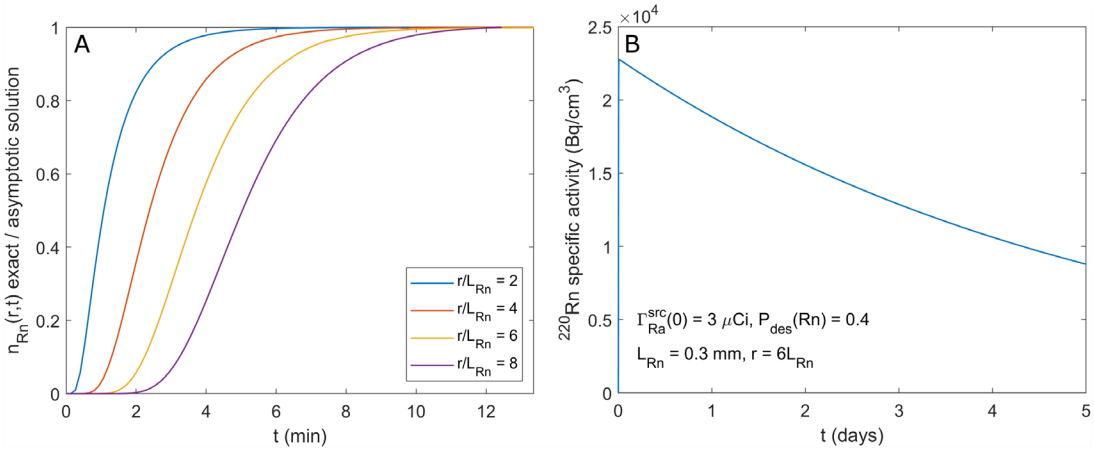

Figure 3. Time-dependent solution for ^{220}Rn, point source geometry. (A) Buildup curves of the exact solution of the time-dependent diffusion equation for ^{220}Rn for the case of a point source. The curves represent the ratio between the exact solution and the asymptotic one, as a function of the time for varying distances from the source, over the first few minutes after source insertion. (B) Specific activity at $r = 6L_{\mathrm{Rn}} = 1.8$ mm as a function of time over several days.

and:

$$A_{\mathrm{Bi}} = \left(\frac{L_{\mathrm{Rn}}^2 L_{\mathrm{Bi}}^2}{L_{\mathrm{Rn}}^2 - L_{\mathrm{Bi}}^2}\right)\frac{\lambda_{\mathrm{Pb}}}{D_{\mathrm{Bi}}}A_{\mathrm{Pb}} \tag{46}$$

$$B_{\mathrm{Bi}} = \left(\frac{L_{\mathrm{Pb}}^2 L_{\mathrm{Bi}}^2}{L_{\mathrm{Pb}}^2 - L_{\mathrm{Bi}}^2}\right)\frac{\lambda_{\mathrm{Pb}}}{D_{\mathrm{Bi}}}B_{\mathrm{Pb}} \tag{47}$$

$$C_{\mathrm{Bi}} = -\left(A_{\mathrm{Bi}} + B_{\mathrm{Bi}}\right). \tag{48}$$

As mentioned in section 4.3, measurements of treated tumor samples, indicate that ^{212}Bi and ^{212}Pb are practically in local secular equilibrium driven by ^{224}Ra. This, in turn, implies $\alpha_{\mathrm{Bi}}/\lambda_{\mathrm{Bi}} \ll 1$, leading us to adopt the assumption $\alpha_{\mathrm{Bi}} = 0$. In appendix B we show that the observation of local secular equilibrium also implies that $L_{\mathrm{Bi}}/L_{\mathrm{Pb}} \lesssim 0.2$ (or less).

6.2. Time-dependent solutions

6.2.1. *^{220}Rn—exact analytical solution*

In appendix C we give a full derivation of the closed-form solution of the time-dependent ^{220}Rn diffusion equation for a point source. The resultant expression is

$$n_{\mathrm{Rn}}(r,t) = \frac{P_{des}(Rn)\,\Gamma_{\mathrm{Ra}}^{src}(0)\,e^{-\lambda_{\mathrm{Ra}}t}}{8\left(\pi D_{\mathrm{Rn}}\right)^{3/2}}\int_0^t \frac{1}{\tau^{3/2}}e^{-\frac{r^2}{4D_{\mathrm{Rn}}\tau}}e^{-(\lambda_{\mathrm{Rn}}-\lambda_{\mathrm{Ra}})\tau}d\tau. \tag{49}$$

As shown in appendix C:

$$\lim_{t\to\infty}\int_0^t \frac{1}{\tau^{3/2}}e^{-\frac{r^2}{4D_{\mathrm{Rn}}\tau}}e^{-(\lambda_{\mathrm{Rn}}-\lambda_{\mathrm{Ra}})\tau}d\tau = \frac{2}{r}\sqrt{\pi D_{\mathrm{Rn}}}e^{-r/L_{\mathrm{Rn}}} \tag{50}$$

such that for $t \gg \tau_{\mathrm{Rn}}$ the exact solution (49) converges to the asymptotic one (37).

Figure 3(A) shows the ratio between the exact and asymptotic solutions as a function of time for several radial distances from the source. The asymptotic solution is attained within minutes over a distance of a few diffusion lengths, with a delay that scales roughly linearly with the distance from the source. Figure 3(B) shows the ^{220}Rn specific activity at $r = 6L_{\mathrm{Rn}}$ for $L_{\mathrm{Rn}} = 0.3$ mm. The source parameters are $\Gamma_{\mathrm{Ra}}^{src}(0) = 3$ μCi (111 kBq) and $P_{des}(\mathrm{Rn}) = 0.4$. The initial buildup of the specific activity is obviously of no practical importance on the time scale relevant for dose calculations (days) and the dose calculation can therefore rely on the asymptotic solution.

6.2.2. *^{212}Pb and ^{212}Bi—exact numerical solution*

The exact time-dependent solutions for ^{212}Pb and ^{212}Bi can found by numerically solving the diffusion-leakage model equations for ^{220}Rn, ^{212}Pb and ^{212}Bi. The solution was obtained here using a one-dimensional computer code (DART1D) developed for this purpose, which employs a fully-implicit scheme with an adaptive time step

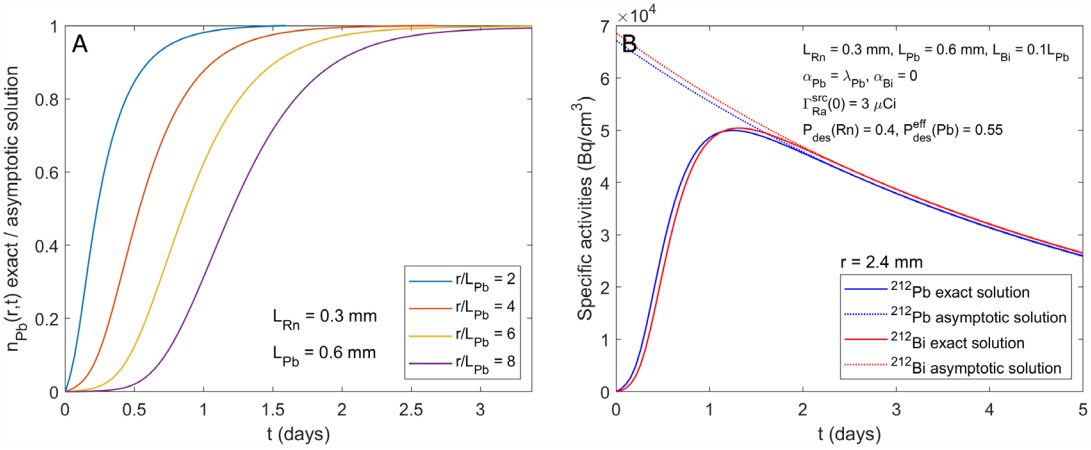

Figure 4. Numerical solutions for the diffusion-leakage equation for ^{212}Pb and ^{212}Bi for the point source geometry. (A) Ratio between the exact solution and the asymptotic one for ^{212}Pb at varying distances from the source as a function of time for $L_{Rn} = 0.3$ mm and $L_{Pb} = 0.6$ mm. (B) Exact and asymptotic solutions for the specific activities of ^{212}Pb and ^{212}Bi at a fixed distance from the source.

that enables calculating both the ^{220}Rn and ^{212}Pb/^{212}Bi transients without resorting to an excessive number of iterations. DART1D will be described in detail in a separate technical note.

Figure 4(A) shows the ratio between the exact and asymptotic solutions for the number density of ^{212}Pb as a function of time for several radial distances from the source. The results are shown for $L_{Rn} = 0.3$ mm and $L_{Pb} = 0.6$ mm. The exact solution converges to the asymptotic one on a scale of several effective ^{212}Pb lifetimes. Similarly to ^{220}Rn the delay in this convergence increases roughly linearly with the radial distance from the source. Figure 4(B) shows the time-dependent specific activities of ^{212}Pb and ^{212}Bi at $r = 4L_{Pb} = 2.4$ mm. Additional parameters in this calculation were $\Gamma^{src}_{Ra}(0) = 3$ μCi (111 kBq), P_{des} (Rn) $= 0.4$, P^{eff}_{des} (Pb) $= 0.55$, P_{leak}(Pb) $= 0.5$ ($\alpha_{Pb} = \lambda_{Pb}$), $L_{Bi} = 0.1L_{Pb}$ and $\alpha_{Bi} = 0$. Unlike the case for ^{220}Rn, the delayed buildup of ^{212}Pb and ^{212}Bi is not negligible, affecting the total dose at a level of ~10%–15% (scale of $\tau^{eff}_{Pb}/\tau_{Ra}$).

7. Macroscopic alpha particle dose for a point source

In this section we use the diffusion-leakage model to estimate the macroscopic alpha particle dose contributed by the diffusing atoms for the case of an ideal point source. We divide the alpha particle dose into two components: the alpha particles emitted by ^{220}Rn and ^{216}Po, at distances which scale with the ^{220}Rn diffusion length, and the alpha particles emitted by ^{212}Bi and ^{212}Po at distances which are governed by the diffusion and leakage of ^{212}Pb (unless $L_{Pb} < L_{Rn}$, in which case the dose scales with the latter). The analysis is limited to alpha particles emitted by the diffusing atoms. Alpha particles emitted directly from the source deposit their entire energy within several dozen micrometers from its surface and are thus of no practical importance in terms of macroscopic dose coverage. We note, however, that the biological effect of the extremely high alpha-particle dose rate on the source surface may warrant further investigations.

7.1. ^{220}Rn/^{216}Po alpha particle dose

The macroscopic alpha particle dose contributed by ^{220}Rn and ^{216}Po from source insertion ($t = 0$) to any particular time t is given by

$$Dose_{\alpha}(\text{RnPo};\,\mathbf{r},t) = \frac{E_{\alpha}(\text{RnPo})}{\rho}\int_0^t \lambda_{Rn} n_{Rn}(\mathbf{r},t')dt' \tag{51}$$

where E_{α}(RnPo) is the total alpha particle energy of ^{220}Rn and ^{216}Po: $E_{\alpha}(\text{RnPo}) = (6.288 + 6.778)$ MeV $=$ 13.066 MeV (Browne 2005, Wu 2007) and ρ is the tissue density. The rationale behind this expression is that the range of alpha particles is much smaller than the diffusion length, and therefore the associated energy depositions occur locally, following the spatial distribution of the ^{220}Rn number density.

We define the asymptotic dose as the dose delivered from source insertion to infinity:

$$Dose^{asy}_{\alpha}(\text{RnPo};\,\mathbf{r}) = \frac{E_{\alpha}(\text{RnPo})}{\rho}\int_0^{\infty} \lambda_{Rn} n_{Rn}(\mathbf{r},t)dt. \tag{52}$$

Because of the short half-life of ^{220}Rn, the ^{220}Rn/^{216}Po alpha particle dose can be calculated to an accuracy of $\sim 10^{-4}$ (in the framework of the diffusion model) by neglecting the initial buildup of ^{220}Rn and assuming that the local ^{220}Rn activity attains its asymptotic form immediately at $t = 0$ throughout the tumor. Thus, using equation (37) for the asymptotic ^{220}Rn number density, we get, for the point source:

$$Dose_{\alpha}(\mathrm{RnPo};\, r, t) = \frac{\lambda_{\mathrm{Rn}} P_{des}(\mathrm{Rn}) \Gamma^{src}_{\mathrm{Ra}}(0) E_{\alpha}(\mathrm{RnPo})}{4\pi\rho D_{\mathrm{Rn}}} \frac{e^{-r/L_{\mathrm{Rn}}}}{r} \tau_{\mathrm{Ra}} \left(1 - e^{-t/\tau_{\mathrm{Ra}}}\right). \tag{53}$$

Asymptotically:

$$Dose^{asy}_{\alpha}(\mathrm{RnPo};\, r) = \frac{\lambda_{\mathrm{Rn}} P_{des}(\mathrm{Rn}) \Gamma^{src}_{\mathrm{Ra}}(0) E_{\alpha}(\mathrm{RnPo})}{4\pi\rho D_{\mathrm{Rn}}} \frac{e^{-r/L_{\mathrm{Rn}}}}{r} \tau_{\mathrm{Ra}}. \tag{54}$$

Throughout the tumor, the ^{220}Rn/^{216}Po alpha particle dose builds up exponentially towards its asymptotic value:

$$\frac{Dose_{\alpha}(\mathrm{RnPo};\, r, t)}{Dose^{asy}_{\alpha}(\mathrm{RnPo};\, r)} = 1 - e^{-t/\tau_{\mathrm{Ra}}}. \tag{55}$$

Thus, within about one week (two ^{224}Ra half-lives), the ^{220}Rn/^{216}Po alpha particle dose reaches 75% of its asymptotic value ($\sim$95% within two weeks), regardless of the distance from the source.

It is instructive to cast equation (54) into a form which conveys its meaning more intuitively. The starting point is to approximate the time dependence of the number density of ^{220}Rn by

$$n^{0D}_{\mathrm{Rn}}(r, t) = \frac{P_{des}(\mathrm{Rn}) \Gamma^{src}_{\mathrm{Ra}}(0)}{4\pi D_{\mathrm{Rn}}} \frac{e^{-r/L_{\mathrm{Rn}}}}{r} \left(e^{-\lambda_{\mathrm{Ra}} t} - e^{-\lambda_{\mathrm{Rn}} t}\right) \tag{56}$$

where we assumed a zero-dimensional picture in which the time dependence is uniform throughout the tumor, similar to equation (23) which includes the initial buildup term. Introducing $n^{0D}_{\mathrm{Rn}}(r, t)$ into the integral in equation (52) and rearranging yields

$$Dose^{asy,0D}_{\alpha}(\mathrm{RnPo};\, r) = P_{des}(\mathrm{Rn}) \Gamma^{src}_{\mathrm{Ra}}(0) \tau_{\mathrm{Ra}} \cdot \frac{E_{\alpha}(\mathrm{RnPo})}{4\pi\rho L^3_{\mathrm{Rn}}} \cdot \frac{e^{-r/L_{\mathrm{Rn}}}}{r/L_{\mathrm{Rn}}}. \tag{57}$$

The first factor in this expression, $P_{des}(\mathrm{Rn})\Gamma^{src}_{\mathrm{Ra}}(0)\tau_{\mathrm{Ra}}$, is the total number of ^{220}Rn atoms released by the source (which is the same as the total number of ^{220}Rn atoms decaying inside the tumor, assuming no ^{220}Rn leakage). The second factor, $E_{\alpha}(\mathrm{RnPo})/(4\pi\rho L^3_{\mathrm{Rn}})$, is a characteristic dose per decay: it is the total alpha particle energy released in the decay of an ^{220}Rn/^{216}Po pair, deposited in a sphere of radius $1.44 L_{\mathrm{Rn}}$. The last factor, $e^{-r/L_{\mathrm{Rn}}}/(r/L_{\mathrm{Rn}})$, provides the spatial dependence of the dose as a function of the radial distance expressed in units of L_{Rn}.

Figure 5(A) shows the asymptotic ^{220}Rn/^{216}Po alpha particle dose as a function of the distance from a point source having an initial ^{220}Rn release rate $S_{\mathrm{Rn}}(0) = P_{des}(\mathrm{Rn})\Gamma^{src}_{\mathrm{Ra}}(0) = 1\ \mu$Ci (37 kBq). The dose is plotted for the two extreme values considered for the ^{220}Rn effective diffusion coefficient: $D_{\mathrm{Rn}} = 0.5 \cdot 10^{-5}$ cm^2 s^{-1} and $D_{\mathrm{Rn}} = 2 \cdot 10^{-5}$ cm^2 s^{-1}, for which the effective diffusion lengths are 0.20 mm and 0.40 mm, respectively. For reference we show the 10 Gy line, as a reasonable value representing therapeutic alpha-particle dose levels. Figure 5(B) shows the diameter of the spherical region receiving an asymptotic dose of 10 Gy, as a function of the initial ^{220}Rn release rate, $S_{\mathrm{Rn}}(0)$, for $0.20 \leqslant L_{\mathrm{Rn}} \leqslant 0.40$ mm (for a point source). The plot was constructed by numerically solving equation (54) for r for a dose of 10 Gy for varying values of $S_{\mathrm{Rn}}(0)$. In both figures, the tissue density was taken as 1.0 g cm^{-3}. Note that, depending on the source activity, therapeutically significant doses are obtained over a region measuring several millimeters in diameter (radial distance of $\sim$5–10 diffusion lengths), even for the case $L_{\mathrm{Rn}} = 0.2$ mm.

7.2. ^{212}Bi/^{212}Po alpha particle dose—numerical solution

Following the same reasoning as for the ^{220}Rn/^{216}Po case, the macroscopic alpha particle dose contributed by ^{212}Bi and ^{212}Po from source insertion to any time t is given by

$$Dose_{\alpha}(\mathrm{BiPo};\, \mathbf{r}, t) = \frac{E_{\alpha}(\mathrm{BiPo})}{\rho} \int_0^t \lambda_{\mathrm{Bi}} n_{\mathrm{Bi}}(\mathbf{r}, t')dt' \tag{58}$$

where $E_{\alpha}(\mathrm{BiPo}) = 7.804$ MeV is the weighted-average energy of the alpha particles emitted by ^{212}Bi and ^{212}Po (Martin 2007). The asymptotic ^{212}Bi/^{212}Po alpha particle dose is

$$Dose^{asy}_{\alpha}(\mathrm{BiPo};\, \mathbf{r}) = \frac{E_{\alpha}(\mathrm{BiPo})}{\rho} \int_0^{\infty} \lambda_{\mathrm{Bi}} n_{\mathrm{Bi}}(\mathbf{r}, t)dt. \tag{59}$$

Because of the delayed buildup of ^{212}Pb throughout the tumor, the asymptotic ^{212}Bi/^{212}Po alpha particle dose should be calculated numerically—by solving the time-dependent diffusion-leakage equations—to pro-

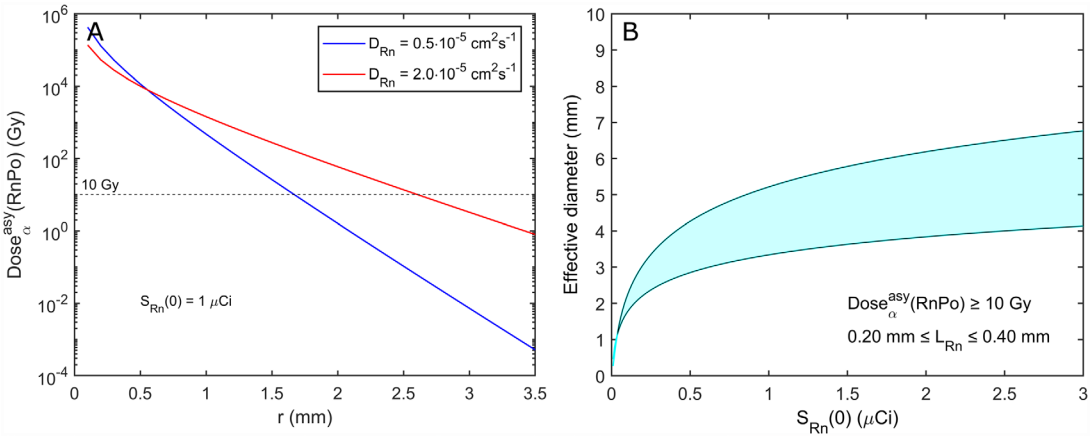

Figure 5. (A) The asymptotic ^{220}Rn/^{216}Po alpha particle dose as a function of the distance from a point source with an initial ^{220}Rn release rate of 1 μCi (37 kBq). The dose is plotted for $D_{Rn} = 2 \cdot 10^{-5}$ cm^2 s^{-1} ($L_{Rn} = 0.40$ mm) and $D_{Rn} = 0.5 \cdot 10^{-5}$ cm^2 s^{-1} ($L_{Rn} = 0.20$ mm). The 10 Gy level is indicated for reference. (B) Diameter of the spherical region receiving an asymptotic ^{220}Rn/^{216}Po alpha particle dose larger than 10 Gy as a function of the initial ^{220}Rn release rate of the (point) source, for the range $0.2 \leqslant L_{Rn} \leqslant 0.4$ mm ($0.5 \cdot 10^{-5} \leqslant D_{Rn} \leqslant 2 \cdot 10^{-5}$ cm^2 s^{-1}).

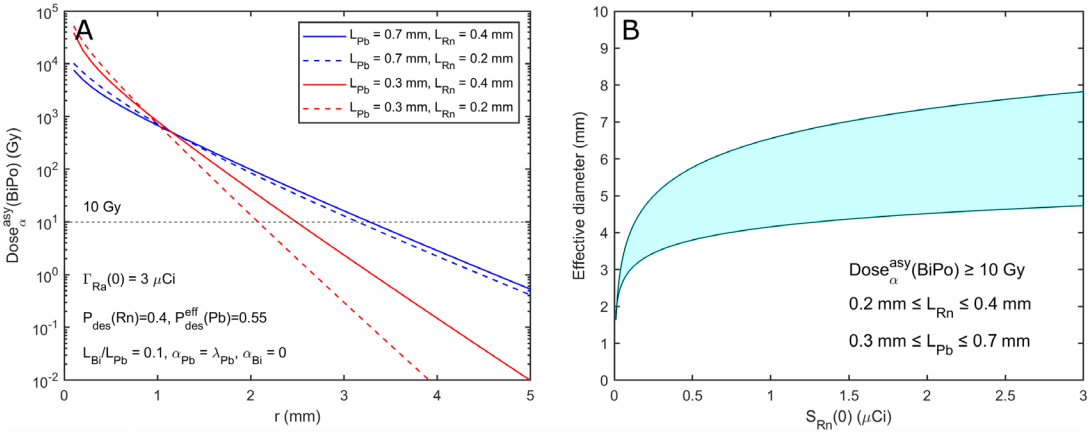

Figure 6. (A) The asymptotic ^{212}Bi/^{212}Po alpha particle dose as a function of the distance from a point source for $L_{Rn} = 0.2,\ 0.4$ mm and $L_{Pb} = 0.3,\ 0.7$ mm, with the other model parameters given in the figure. The 10 Gy level is shown for reference. (B) Diameter of the spherical region receiving an asymptotic ^{212}Bi/^{212}Po alpha particle dose larger than 10 Gy as a function of the initial ^{220}Rn release rate of the (point) source, for the range $0.2 \leqslant L_{Rn} \leqslant 0.4$ mm, $0.3 \leqslant L_{Pb} \leqslant 0.7$ mm. The remaining model parameters are the same as in (A).

duce accurate results (an approximate method to calculate the dose is discussed below). Figure 6(A) shows the asymptotic ^{212}Bi/^{212}Po dose as a function of the distance from a point source with $\Gamma^{src}_{Ra}(0) = 3$ μCi (111 kBq), $P_{des}(\mathrm{Rn}) = 0.4$ and $P^{eff}_{des}(\mathrm{Pb}) = 0.55$. We keep the same choice of model parameters as before: $\alpha_{Pb} = \lambda_{Pb}$, $\alpha_{Bi} = 0$ and $L_{Bi} = 0.1L_{Pb}$, leaving L_{Rn} and L_{Pb} as adjustable parameters. For ^{220}Rn, we continue using the range $0.2 \leqslant L_{Rn} \leqslant 0.4$ mm. For ^{212}Pb, we consider the range $0.3 \leqslant L_{Pb} \leqslant 0.7$ mm. Figure 6(A) thus contains 4 curves, corresponding to $L_{Rn} = 0.2,\ 0.4$ mm and $L_{Pb} = 0.3,\ 0.7$ mm. As could be expected, the dose profile is more sensitive to changes in the ^{220}Rn effective diffusion length when the effective ^{212}Pb diffusion length is small. Figure 6(B) shows the dependence of the diameter of the spherical region in which the ^{212}Bi/^{212}Po dose exceeds 10 Gy (for the same range of ^{220}Rn and ^{212}Pb effective diffusion lengths) on the initial release rate of ^{220}Rn from the source, assuming the same desorption probabilities as in figure 6(A). Comparing figures 5 and 6, it is evident that for the range of model parameters under consideration, the ^{212}Bi/^{212}Po dose extends over a larger region than that covered by ^{220}Rn and ^{216}Po.

7.3. ^{212}Bi/^{212}Po alpha particle dose—approximate solution

A simple approximation to the ^{212}Bi/^{212}Po alpha particle dose can be made by assuming that the local ^{212}Bi activity throughout the tumor can be factorized into a pure space-dependent part and a pure time-dependent part, similarly to the zero-dimensional approximation for ^{220}Rn, equation (56). The space-dependent part is taken to be the same as that of the asymptotic ^{212}Bi function, given—for the case of a point source—in equation (44).

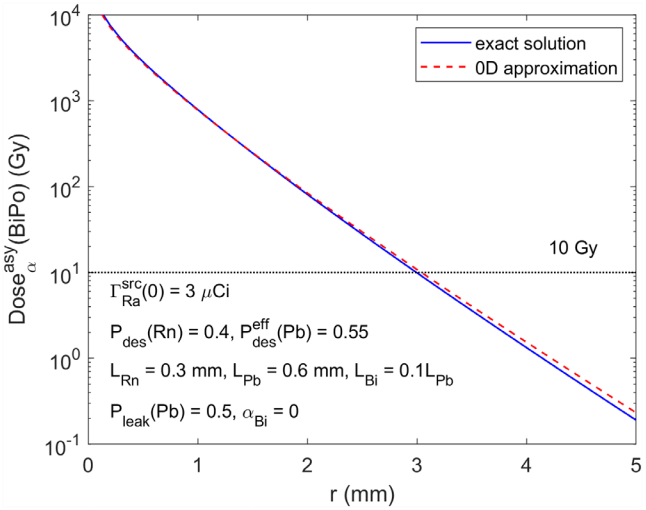

Figure 7. Comparison between the 0D approximation for the ^{212}Bi/^{212}Po alpha particle dose and the exact solution (point source geometry).

The time-dependent part is taken as that of the total ^{212}Pb activity inside the tumor, equation (27). Under this approximation, the local ^{212}Bi activity (for the case of a point source) is given by

$$\lambda_{Bi} n^{0D}_{Bi}(r,t) = \lambda_{Bi}\left(A_{Bi}\frac{e^{-r/L_{Rn}}}{r} + B_{Bi}\frac{e^{-r/L_{Pb}}}{r} + C_{Bi}\frac{e^{-r/L_{Bi}}}{r}\right) \cdot \left(e^{-\lambda_{Ra}t} - e^{-(\lambda_{Pb}+\alpha_{Pb})t}\right) \tag{60}$$

where the coefficients A_{Bi}, B_{Bi} and C_{Bi} are given in equation (46)–(48). The asymptotic dose is then

$$Dose^{0D,asy}_{\alpha}(\text{BiPo};\, r) = \frac{E_{\alpha}(\text{BiPo})}{\rho}\lambda_{Bi} \cdot \left(A_{Bi}\frac{e^{-r/L_{Rn}}}{r} + B_{Bi}\frac{e^{-r/L_{Pb}}}{r} + C_{Bi}\frac{e^{-r/L_{Bi}}}{r}\right)\left(\tau_{Ra} - \tau^{eff}_{Pb}\right). \tag{61}$$

Figure 7 shows a comparison between the exact and approximate solutions for the ^{212}Bi/^{212}Po asymptotic alpha particle dose, for a representative case of the model parameters. The 0D approximation is within 5%–10% of the exact solution for $r \sim 2$–3 mm (but overestimates it by up to $\sim$20% at $r = 5$ mm).

Assuming the 0D temporal behavior, in the limit $L_{Rn}, L_{Bi} \ll L_{Pb}$ one obtains the intuitive expression:

$$Dose^{0D,asy}_{\alpha}(\text{BiPo};\, r) \approx [1 - P_{leak}(\text{Pb})]\, P^{eff}_{des}(\text{Pb})\Gamma^{src}_{Ra}(0)\tau_{Ra} \cdot \frac{E_{\alpha}(\text{BiPo})}{4\pi\rho L^3_{Pb}} \cdot \frac{e^{-r/L_{Pb}}}{r/L_{Pb}}. \tag{62}$$

This expression is analogous to the one obtained above for the ^{220}Rn/^{216}Po dose, eq. (57). The first factor, $[1 - P_{leak}(\text{Pb})]\, P^{eff}_{des}(\text{Pb})\Gamma^{src}_{Ra}(0)\tau_{Ra}$, is the total number of ^{212}Pb atoms released by the source which decay inside the tumor. Assuming no independent leakage of ^{212}Bi, this is equal to the total number of alpha decays of ^{212}Bi and ^{212}Po inside the tumor. The second and third factors are similar in their meaning to the ones appearing in the expression for the ^{220}Rn/^{216}Po dose.

7.4. ^{220}Rn/^{216}Po and ^{212}Bi/^{212}Po alpha particle dose combined

The overall asymptotic macroscopic alpha particle dose, comprising the contributions from ^{220}Rn/^{216}Po and ^{212}Bi/^{212}Po is shown in figure 8 for the range $0.2 \leqslant L_{Rn} \leqslant 0.4$ mm and $0.3 \leqslant L_{Pb} \leqslant 0.7$ mm. The other model parameters are the same as those used before. The shaded region represents the range of possible values for the total dose. The blue line shows the specific case $L_{Rn} = 0.3$ mm and $L_{Pb} = 0.6$ mm (characteristic of murine SCC).

The region where the overall alpha particle dose is close to $\sim$10 Gy (several ^{212}Pb diffusion lengths away from the source) is the most critical one in terms of treatment planning. At shorter distances cell killing is trivially guaranteed by dose levels of the order of several dozen Gy, leading, on average, to several dozen alpha particle hits to cell nuclei of typical sizes. Farther away (where the dose is of order of $\sim$1 Gy), statistical fluctuations in the number of alpha particle hits to cell nuclei are large, leading to partial cell killing. A detailed study on the relation between the macroscopic alpha particle dose and the microdosimetric aspects of the problem will be discussed

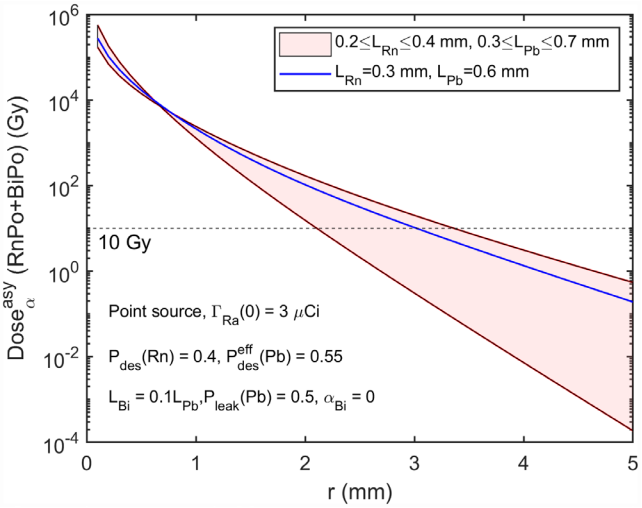

Figure 8. Total asymptotic alpha particle dose for a point source, comprising contributions from ^{220}Rn/^{216}Po and ^{212}Bi/^{212}Po. The shaded region represents the dose for for $0.2 \leqslant L_{\mathrm{Rn}} \leqslant 0.4$ mm, $0.3 \leqslant L_{\mathrm{Pb}} \leqslant 0.7$ mm and the blue line the case $L_{\mathrm{Rn}} = 0.3$ mm and $L_{\mathrm{Pb}} = 0.6$ mm. The source parameters and other model parameters are given in the figure.

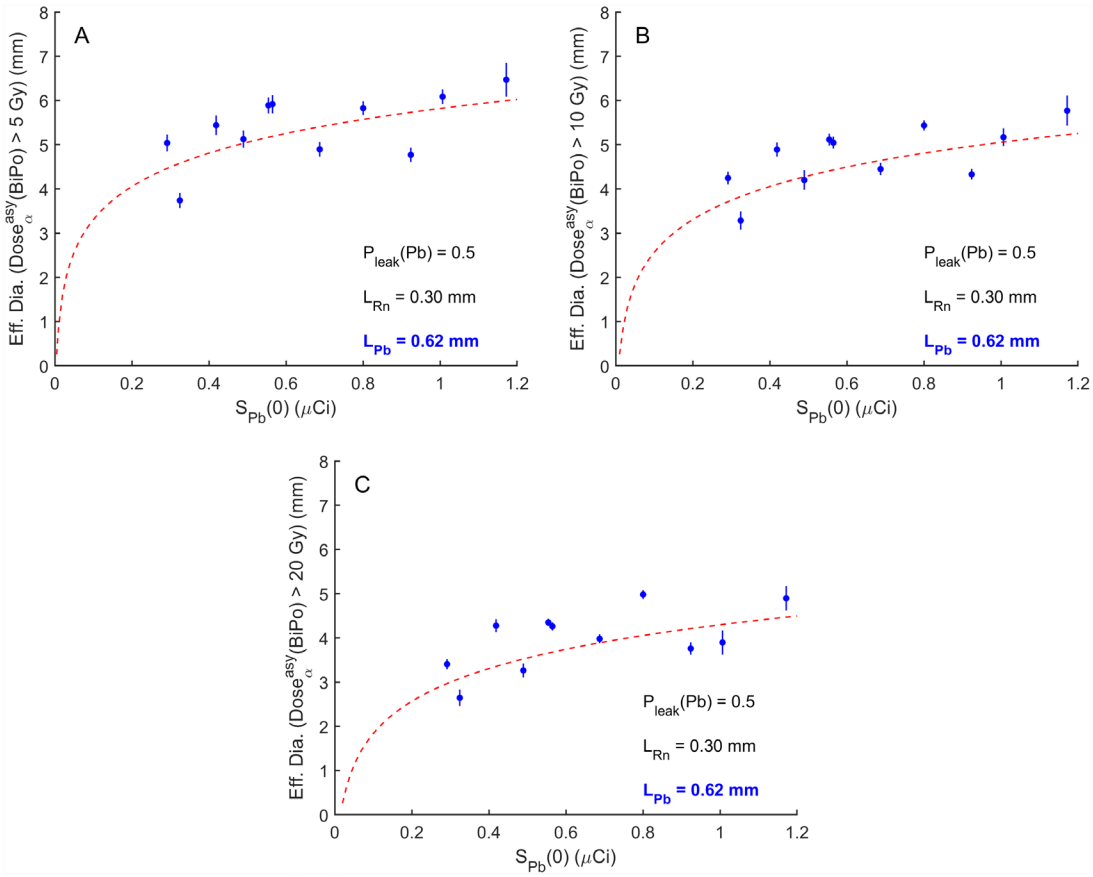

Figure 9. Autoradiography data from murine SCC tumors: effective diameters corresponding to a macroscopic ^{212}Bi/^{212}Po alpha particle dose of 5,10 and 20 Gy as a function of the initial ^{212}Pb release rate from the source. The data are fitted with the diffusion-leakage model, keeping $P_{leak} = 0.5$ and $L_{\mathrm{Rn}} = 0.3$ mm, resulting in a best fit value of $L_{\mathrm{Pb}} = 0.62$ mm.

in a separate publication, relying on established methodologies such as those described, for example, in MIRD Pamphlet 22 (Sgouros *et al* 2010).

7.5. Example: estimating the model parameters for murine SCC tumors

A detailed description of several complementary methodologies employed to estimate the diffusion-leakage model parameters in mice tumors will be given in a separate publication. Here we show, as an example, a particular

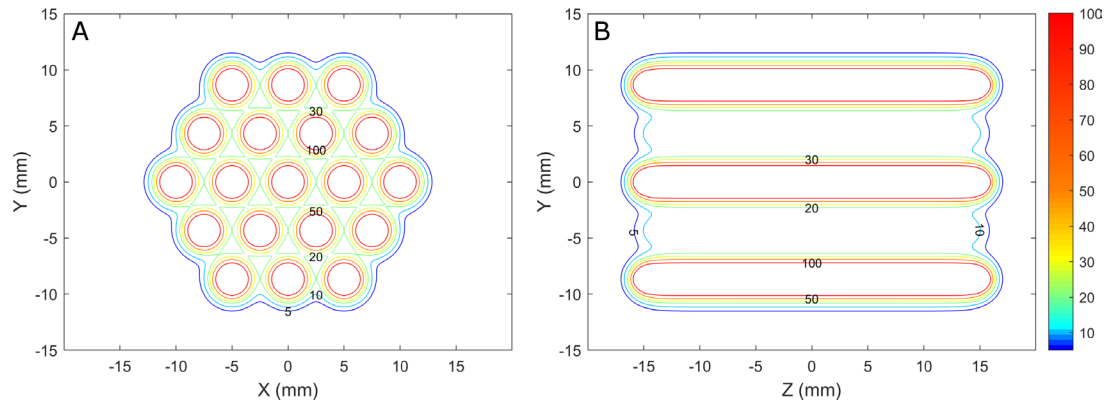

Figure 10. Asymptotic alpha particle dose for an hexagonal array of line sources. The sources are 3 cm long and carry 3 μCi ^{224}Ra per cm. Source spacing is 5 mm. The desorption probabilities are the same as in previous figures. The model parameters are $L_{\mathrm{Rn}} = 0.3$ mm, $L_{\mathrm{Pb}} = 0.6$ mm, $L_{\mathrm{Bi}} = 0.1L_{\mathrm{Pb}}$, $P_{leak}(\mathrm{Pb}) = 0.5$, $\alpha_{\mathrm{Bi}} = 0$. The dose was calculated using the 0D approximation. (A) Isodose curves in the mid-plane of the array ($z = 0$); (B) isodose curves in the $x = 0$ plane.

analysis of murine SCC data. The autoradiography procedure was previously described in Arazi *et al* (2007). Briefly, two-dimensional images of ^{212}Pb activity distributions in histological sections taken perpendicularly to the source and close to its mid plane, are translated to estimates of the macroscopic ^{212}Bi/^{212}Po alpha particle dose. For a given dose D_0, we calculate the area of the section subject to higher or equal dose levels $A(dose \geqslant D_0)$, and define the corresponding effective diameter as $D_{eff}(dose \geqslant D_0) = 2\sqrt{A(dose \geqslant D_0)/\pi}$. Figure 9 shows the measured effective diameter for $Dose_{\alpha}^{asy}(\mathrm{BiPo}) = 5, 10, 20$ Gy as a function of $S_{\mathrm{Pb}}(0) = P_{des}^{eff}(\mathrm{Pb})\Gamma_{\mathrm{Ra}}^{src}(0)$, for 11 murine SCC tumors (SQ2 cell line). Error bars represent systematic uncertainties related to the image processing method. The entire dataset is fitted by a numerical calculation of the ^{212}Bi/^{212}Po dose in the mid plane of the source, with L_{Pb} as the free parameter, for $P_{leak}(\mathrm{Pb}) = 0.5$ and $L_{\mathrm{Rn}} = 0.3$ mm (for simplicity we assumed $L_{\mathrm{Bi}} \ll L_{\mathrm{Pb}}$). The best fit value is $L_{\mathrm{Pb}} = 0.62$ mm. Varying the parameters over the ranges $0.3 \leqslant P_{leak}(\mathrm{Pb}) \leqslant 0.7$ and $0.2 \leqslant L_{\mathrm{Rn}} \leqslant 0.4$ mm yields $0.49 \leqslant L_{\mathrm{Pb}} \leqslant 0.84$ mm (but with considerably better fit quality for values close the the center of these intervals). Keeping $P_{leak}(\mathrm{Pb}) = 0.5$ with both L_{Rn} and L_{Pb} as free parameters gives $L_{\mathrm{Rn}} = 0.48$ mm and $L_{\mathrm{Pb}} = 0.55$ mm. Scanning the range $0.3 \leqslant P_{leak}(\mathrm{Pb}) \leqslant 0.7$ gives $0.43 \leqslant L_{\mathrm{Rn}} \leqslant 0.55$ mm and $0.48 \leqslant L_{\mathrm{Pb}} \leqslant 0.71$ mm. Other analysis methods lead to similar values for L_{Pb}.

7.6. Example of an array of line sources

A systematic parametric study of arrays of DaRT sources will be dealt with in a subsequent publications. As an example, we show in figure 10 the case of an hexagonal array of 3 cm long line sources spaced 5 mm apart, each carrying 3 μCi ^{224}Ra per cm, with $P_{des}(\mathrm{Rn}) = 0.4$ and $P_{des}^{eff}(\mathrm{Pb}) = 0.55$. The diffusion lengths are $L_{\mathrm{Rn}} = 0.3$ mm and $L_{\mathrm{Pb}} = 0.6$ mm. The ^{212}Pb leakage probability is taken as 50%, $L_{\mathrm{Bi}} = 0.1L_{\mathrm{Pb}}$ and $\alpha_{\mathrm{Bi}} = 0$. The total alpha particle dose (sum of all contributions) was calculated using the 0D approximation, by dividing the sources to point-like increments and summing the contribution of all sources at each point. Panel A shows the dose in the mid-plane of the sources ($z = 0$), while panel B shows the dose in a plane parallel to the sources and passing thorough the center of the array ($x = 0$). The minimal dose between sources is 14 Gy.

8. Summary and discussion

DaRT is a radically new form of radiation therapy, which allows, for the first time, the treatment of solid tumors by alpha particles. After years of extensive preclinical investigations, it has recently reached clinical trials with promising results, as reported in Popovtzer *et al* (2019). Its main advantages are the ability to deliver a lethal alpha particle dose to the tumor without risking adjacent critical structures, the efficacy of alpha radiation against hypoxic and radiation-resistant cancer cells, and the rapid shrinkage of treated tumors (on the scale of days). DaRT has so far been tested clinically as a stand-alone treatment, but can also be combined with systemic therapy (in particular, immunotherapy) or with conventional radiation (for example as a boost to external beam radiation therapy).

DaRT dosimetry is challenging because of the complex and dynamic nature of the tumor tissue through which the alpha-emitting atoms migrate. A complete description of the problem on a patient- and tumor-specific basis will require detailed spatial and temporal information which is presently unattainable in clinical set-

tings. This calls for the development of practical modeling techniques that can provide an approximate quantitative starting point for treatment planning.

The diffusion-leakage model introduced in this work is a first step in this direction. While being highly simplistic (assuming the medium is homogeneous, isotropic and time-independent), it constitutes a zero-order approximate framework which allows for gross macroscopic dose estimates. Importantly, the activity and spacing of the sources used in the SCC clinical trial were set based on the predictions of the model, with parameters extracted from animal studies. The promising outcomes of the trial, where essentially all treated tumors responded by drastic shrinking within days after the treatment, indicate that the approach presented here can indeed provide a meaningful base for further development.

Much additional work is required to expand the physical basis for DaRT dosimetry. This includes extensive measurements of the model parameters in other (non-SCC) tumor types; investigation of convective and nonlinear effects in treated tumors; microdosimetry simulations augmented by detailed *in vitro* studies, to understand the relation between the macroscopic alpha particle dose and cell survival; studies on establishing correlations between observables accessible by medical imaging and local tissue parameters affecting the spread of alpha-emitters; studies on tumor shrinkage rate and its effect on the overall dose, and the development of *in vivo* probes to locally measure the alpha particle dose in preclinical and clinical settings.

One can hope that the knowledge and experience that will be gained in these studies, as well as in ongoing and planned clinical trials, will bring DaRT treatment-planning closer to the present degree of confidence of photon-based radiation therapy, allowing for effective utilization of the many advantages offered by this method.

Acknowledgments

The author would like to thank Prof Itzhak Kelson for his thoughtful comments on this manuscript. The author is a share holder in Alpha TAU Medical Ltd. and has a research grant from the company.

Appendix A. Experimental determination of the ^{220}Rn and ^{212}Pb desorption probabilities

A.1. ^{220}Rn

The measurement setup is based on a silicon charged particle detector (model ULTRA, EG&G ORTEC) and auxiliary electronics. Data are read to a PC-based multichannel analyzer. The setup enables the measurement of alpha particle energy spectra with a resolution of 2.5 keV/channel and a typical alpha-line FWHM of 20 keV. The detector is mounted inside a vacuum chamber, whose outlet is connected to a rotary pump. A needle valve controls air inlet. The detector has a circular aperture with an active area of 150 mm^2. The DaRT source is mounted vertically on a rotating device positioned opposite to the detector to obtain the time average of the activity distributed on its surface. The ^{224}Ra activity and ^{220}Rn desorption probability are determined based on the 5685 keV line (95%) of ^{224}Ra and the 6288 keV line (100%) of ^{220}Rn. The detection efficiency of the setup is calculated based on its geometry to an accuracy of $\sim$2%, which also sets the accuracy of the activity measurement. Usually, spectral measurements of alpha emitting samples are performed in vacuum, to avoid modifications of the energy spectrum. In our case, in order to determine the ^{220}Rn desorption probability, the measurement is performed at low pressure under continuous air flow, which takes the ^{220}Rn atoms emitted from the source out of the measurement chamber. The pressure level (about 5 mbar), adjusted by the inlet needle valve, was set to prevent the emitted ^{220}Rn atoms from being stuck in the chamber walls and on the detector itself. The flow rate is sufficient to replace all chamber gas within about one second. Thus, in an obtained spectrum, the ^{220}Rn line is comprised of alpha particles arriving at the detector only from the source, and the ^{220}Rn desorption probability is given by

$$P_{des}(\mathrm{Rn}) = 1 - \frac{\Gamma^{src}_{\mathrm{Rn}}}{\Gamma^{src}_{\mathrm{Ra}}} \tag{A.1}$$

where $\Gamma^{src}_{\mathrm{Ra}}$ and $\Gamma^{src}_{\mathrm{Rn}}$ are the respective source activities of ^{224}Ra and ^{220}Rn. Typical values are $P_{des}(\mathrm{Rn}) \sim (40 \pm 4)\%$.

A.2. ^{212}Pb

Since ^{220}Rn is a noble gas, its release rate from the source does not depend on the medium in which the source is placed. Therefore, its desorption probability can be determined in low pressure gas, being the same as in tissue. The situation is different for ^{212}Pb, as its desorption probability is much higher in gas than in tissue. The reason is that in gas ^{220}Rn, ^{216}Po and ^{212}Pb are emitted by recoil and cannot return to the source surface. On the other hand, in tissue, the recoiling positive ions stop within a few nm from the surface, and can drift back to it. While ^{220}Rn ions returning to the surface are neutralized on it and diffuse back into the tissue, returning ^{216}Po and ^{212}Pb ions may bind to it. Therefore, in order to correctly determine the desorption probability of ^{212}Pb, one should

place the source inside tissue or a medium with similar properties (such as serum). The ^{212}Pb activity inside the medium is given by

$$\Gamma_{\mathrm{Pb}}^{med}(t) = \frac{\lambda_{\mathrm{Pb}}}{\lambda_{\mathrm{Pb}} - \lambda_{\mathrm{Ra}}} P_{des}^{eff}(\mathrm{Pb}) \Gamma_{\mathrm{Ra}}^{src}(0) \left(e^{-\lambda_{\mathrm{Ra}} t} - e^{-\lambda_{\mathrm{Pb}} t}\right) \tag{A.2}$$

where $t = 0$ is the time of source placement inside the medium. Knowing the ^{224}Ra activity at $t = 0$ and measuring the ^{212}Pb activity inside the medium one can then obtain $P_{des}^{eff}(\mathrm{Pb})$ from equation (A.2). In practice, measurements are performed using a small amount ($\sim$1 ml) of serum in a vial placed inside a NaI(Tl) well-type gamma spectrometer of known efficiency, and the ^{212}Pb activity is determined from its photopeak at 239 keV (43.6%). An alternative approach, required in cases where the medium is a live tissue and ^{212}Pb leakage through the blood must be considered, is to find $P_{des}^{eff}(\mathrm{Pb})$ by measuring the ^{212}Pb activity on the source after its extraction from the sample. In this case, one should take into consideration a contribution from the 241 keV line of ^{224}Ra (4.1%) to the ^{212}Pb photopeak, and apply a bi-exponential fit to the time-dependent count rate to account for the evolution of both isotopes. Typical measured values are $P_{des}^{eff}(\mathrm{Pb}) \sim 55 \pm 5\%$.

Appendix B. Derivation of the asymptotic solutions to the time-dependent diffusion-leakage model

B.1. ^{220}Rn

We consider the case of a point source of ^{224}Ra in an infinite homogeneous medium. In spherical coordinates, the time-dependent ^{220}Rn diffusion equation (13) becomes

$$\frac{\partial n_{\mathrm{Rn}}}{\partial t} = \frac{D_{\mathrm{Rn}}}{r^2} \frac{\partial}{\partial r}\left(r^2 \frac{\partial n_{\mathrm{Rn}}}{\partial r}\right) + s_{\mathrm{Rn}} - \lambda_{\mathrm{Rn}} n_{\mathrm{Rn}} \tag{B.1}$$

where the source term is $s_{\mathrm{Rn}}(r,t) = P_{des}(Rn)\,\Gamma_{\mathrm{Ra}}^{src}(0)\,e^{-\lambda_{\mathrm{Ra}} t}\delta(r)$. For $t \gg \tau_{\mathrm{Rn}}$ (i.e. at times larger than a few minutes), substituting the asymptotic form $n_{\mathrm{Rn}}^{asy}(r,t) = \widetilde{n}_{\mathrm{Rn}}(r)\,e^{-\lambda_{\mathrm{Ra}} t}$ gives, for $r > 0$:

$$\frac{1}{r^2}\frac{d}{dr}\left(r^2 \frac{d\widetilde{n}_{\mathrm{Rn}}}{dr}\right) - \frac{1}{L_{\mathrm{Rn}}^2}\widetilde{n}_{\mathrm{Rn}} = 0 \tag{B.2}$$

where we used the definition of the effective ^{220}Rn diffusion length:

$$L_{\mathrm{Rn}} = \sqrt{\frac{D_{\mathrm{Rn}}}{\lambda_{\mathrm{Rn}} - \lambda_{\mathrm{Ra}}}}. \tag{B.3}$$

The solution for equation (B.2) requires a change of variables. We substitute $\widetilde{n}_{\mathrm{Rn}} = \frac{w}{r}$, leading to

$$\frac{d^2 w}{dr^2} - \frac{1}{L_{\mathrm{Rn}}^2} w = 0. \tag{B.4}$$

The general solution for this equation is $w = A_{\mathrm{Rn}} e^{-r/L_{\mathrm{Rn}}} + B_{\mathrm{Rn}} e^{r/L_{\mathrm{Rn}}}$. Since the second term diverges for $r \to \infty$, $B_{\mathrm{Rn}} = 0$ and thus

$$\widetilde{n}_{\mathrm{Rn}} = \frac{A_{\mathrm{Rn}} e^{-r/L_{\mathrm{Rn}}}}{r}. \tag{B.5}$$

The coefficient A_{Rn} is found using the boundary condition at $r \to 0$:

$$\lim_{r\to 0} 4\pi r^2 j_{\mathrm{Rn}}^{asy}(r,t) = P_{des}(Rn)\,\Gamma_{\mathrm{Ra}}^{src}(0)\,e^{-\lambda_{\mathrm{Ra}} t}. \tag{B.6}$$

The radial component of the asymptotic current density, j_{Rn}^{asy} is given by

$$j_{\mathrm{Rn}}^{asy}(r,t) = -D_{\mathrm{Rn}} \frac{\partial n_{\mathrm{Rn}}^{asy}}{\partial r} = \frac{D_{\mathrm{Rn}} A_{\mathrm{Rn}}}{r^2} e^{-r/L_{\mathrm{Rn}}} \left(1 + \frac{r}{L_{\mathrm{Rn}}}\right) e^{-\lambda_{\mathrm{Ra}} t}. \tag{B.7}$$

Substituting result (B.7) in the boundary condition (B.6), gives

$$A_{\mathrm{Rn}} = \frac{P_{des}(Rn)\,\Gamma_{\mathrm{Ra}}^{src}(0)}{4\pi D_{\mathrm{Rn}}} \tag{B.8}$$

and hence

$$n_{\mathrm{Rn}}^{asy}(r,t) = \frac{P_{des}(Rn)\,\Gamma_{\mathrm{Ra}}^{src}(0)\,e^{-\lambda_{\mathrm{Ra}} t}}{4\pi D_{\mathrm{Rn}}} \frac{e^{-r/L_{\mathrm{Rn}}}}{r}. \tag{B.9}$$

B.2. ^{212}Pb

The time-dependent diffusion-leakage equation for ^{212}Pb in spherical coordinates is

$$\frac{\partial n_{\mathrm{Pb}}}{\partial t} = \frac{D_{\mathrm{Pb}}}{r^2}\frac{\partial}{\partial r}\left(r^2\frac{\partial n_{\mathrm{Pb}}}{\partial r}\right) + s_{\mathrm{Pb}} - \left(\lambda_{\mathrm{Pb}} + \alpha_{\mathrm{Pb}}\right) n_{\mathrm{Pb}}. \tag{B.10}$$

The source term s_{Pb} in equation (B.10) can be written as

$$s_{\mathrm{Pb}}\left(r,t\right) = \lambda_{\mathrm{Rn}} n_{\mathrm{Rn}} + \left(P_{des}^{eff}\left(Pb\right) - P_{des}\left(Rn\right)\right)\Gamma_{\mathrm{Ra}}^{src}\left(0\right)e^{-\lambda_{\mathrm{Ra}}t}\delta\left(r\right). \tag{B.11}$$

The boundary condition at $r \to 0$ is

$$\lim_{r\to 0} 4\pi r^2 j_{\mathrm{Pb}}\left(r,t\right) = \left(P_{des}^{eff}\left(Pb\right) - P_{des}\left(Rn\right)\right)\Gamma_{\mathrm{Ra}}^{src}\left(0\right)e^{-\lambda_{\mathrm{Ra}}t}. \tag{B.12}$$

The first step in the asymptotic analysis for ^{212}Pb is substituting the asymptotic forms, equations (34) and (35) in the diffusion-leakage equation (B.10). For $r > 0$ this gives

$$-\lambda_{\mathrm{Ra}}\widetilde{n}_{\mathrm{Pb}} = \frac{D_{\mathrm{Pb}}}{r^2}\frac{d}{dr}\left(r^2\frac{d\widetilde{n}_{\mathrm{Pb}}}{dr}\right) - \left(\lambda_{\mathrm{Pb}} + \alpha_{\mathrm{Pb}}\right)\widetilde{n}_{\mathrm{Pb}} + \lambda_{\mathrm{Rn}}\widetilde{n}_{\mathrm{Rn}}. \tag{B.13}$$

Substituting the asymptotic result for ^{220}Rn and rearranging gives

$$\frac{1}{r^2}\frac{d}{dr}\left(r^2\frac{d\widetilde{n}_{\mathrm{Pb}}}{dr}\right) - \frac{1}{L_{\mathrm{Pb}}^2}\widetilde{n}_{\mathrm{Pb}} + \frac{\lambda_{\mathrm{Rn}}}{D_{\mathrm{Pb}}}A_{\mathrm{Rn}}\frac{e^{-r/L_{\mathrm{Rn}}}}{r} = 0 \tag{B.14}$$

where we used the definition of the effective ^{212}Pb diffusion length:

$$L_{\mathrm{Pb}} = \sqrt{\frac{D_{\mathrm{Pb}}}{\lambda_{\mathrm{Pb}} + \alpha_{\mathrm{Pb}} - \lambda_{\mathrm{Ra}}}}. \tag{B.15}$$

We now attempt a solution of the form

$$\widetilde{n}_{\mathrm{Pb}}\left(r\right) = A_{\mathrm{Pb}}\frac{e^{-r/L_{\mathrm{Rn}}}}{r} + B_{\mathrm{Pb}}\frac{e^{-r/L_{\mathrm{Pb}}}}{r}. \tag{B.16}$$

When this solution is inserted into equation (B.14) the terms comprising $\frac{e^{-r/L_{\mathrm{Pb}}}}{r}$ cancel out and we get

$$\begin{aligned} A_{\mathrm{Pb}} &= \left(\frac{L_{\mathrm{Rn}}^2 L_{\mathrm{Pb}}^2}{L_{\mathrm{Rn}}^2 - L_{\mathrm{Pb}}^2}\right)\frac{\lambda_{\mathrm{Rn}}}{D_{\mathrm{Pb}}}A_{\mathrm{Rn}} \\ &= \left(\frac{L_{\mathrm{Rn}}^2 L_{\mathrm{Pb}}^2}{L_{\mathrm{Rn}}^2 - L_{\mathrm{Pb}}^2}\right)\frac{\lambda_{\mathrm{Rn}}}{D_{\mathrm{Pb}}}\frac{P_{des}\left(Rn\right)\Gamma_{\mathrm{Ra}}^{src}\left(0\right)}{4\pi D_{\mathrm{Rn}}}. \end{aligned} \tag{B.17}$$

The second coefficient, B_{Pb}, is found from the boundary condition (B.12). The radial component of the current density is

$$\begin{aligned} j_{\mathrm{Pb}}\left(r,t\right) &= -D_{\mathrm{Pb}}\frac{\partial n_{\mathrm{Pb}}}{\partial r} \\ &= \frac{D_{\mathrm{Pb}}e^{-\lambda_{\mathrm{Ra}}t}}{r^2}\left(A_{\mathrm{Pb}}e^{-r/L_{\mathrm{Rn}}}\left(1 + \frac{r}{L_{\mathrm{Rn}}}\right) + B_{\mathrm{Pb}}e^{-r/L_{\mathrm{Pb}}}\left(1 + \frac{r}{L_{\mathrm{Pb}}}\right)\right). \end{aligned} \tag{B.18}$$

Inserting this into the boundary condition and taking the limit $r \to 0$ gives

$$B_{\mathrm{Pb}} = \frac{\left(P_{des}^{eff}\left(Pb\right) - P_{des}\left(Rn\right)\right)\Gamma_{\mathrm{Ra}}^{src}\left(0\right)}{4\pi D_{\mathrm{Pb}}} - A_{\mathrm{Pb}}. \tag{B.19}$$

Thus

$$n_{\mathrm{Pb}}^{asy}\left(r,t\right) = \left(A_{\mathrm{Pb}}\frac{e^{-r/L_{\mathrm{Rn}}}}{r} + B_{\mathrm{Pb}}\frac{e^{-r/L_{\mathrm{Pb}}}}{r}\right)e^{-\lambda_{\mathrm{Ra}}t} \tag{B.20}$$

where A_{Pb} and B_{Pb} are given by equations (B.17) and (B.19).

B.3. ^{212}Bi

The diffusion-leakage equation for ^{212}Bi in spherical coordinates is

$$\frac{\partial n_{\mathrm{Bi}}}{\partial t} = \frac{D_{\mathrm{Bi}}}{r^2}\frac{\partial}{\partial r}\left(r^2\frac{\partial n_{\mathrm{Bi}}}{\partial r}\right) - \left(\lambda_{\mathrm{Bi}} + \alpha_{\mathrm{Bi}}\right) n_{\mathrm{Bi}} + \lambda_{\mathrm{Pb}} n_{\mathrm{Pb}}. \tag{B.21}$$

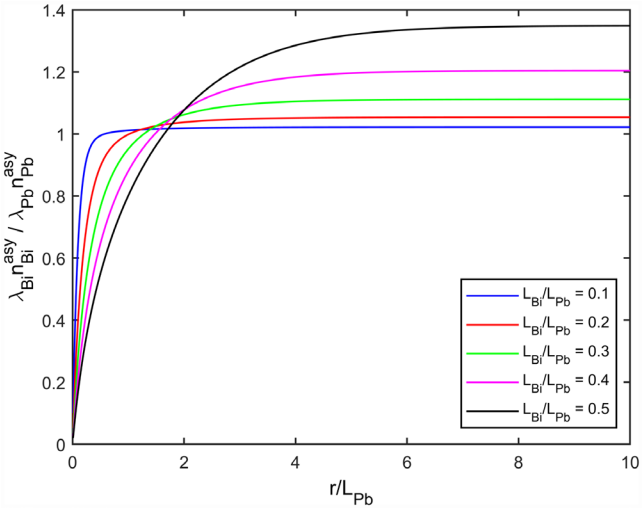

Figure B1. The local asymptotic ^{212}Bi/^{212}Pb activity ratio predicted by the diffusion-leakage model as a function of the radial distance from the (point) source, for varying values for $L_{\mathrm{Bi}}/L_{\mathrm{Pb}}$. The calculation assumed $\alpha_{\mathrm{Bi}} = 0$ and $\alpha_{\mathrm{Pb}} = \lambda_{\mathrm{Pb}}$. The distance from the source is expressed in units of L_{Pb}.

Since there is no direct release of ^{212}Bi from the source, the boundary condition at $r \to 0$ is

$$\lim_{r\to 0} 4\pi r^2 j_{\mathrm{Bi}} = 0. \tag{B.22}$$

Substituting into equation (B.21) the asymptotic form $n_{\mathrm{Bi}}^{asy}(r,t) = \widetilde{n}_{\mathrm{Bi}}(r)\, e^{-\lambda_{\mathrm{Ra}} t}$, yields

$$\frac{1}{r^2}\frac{d}{dr}\left(r^2 \frac{d\widetilde{n}_{\mathrm{Bi}}}{dr}\right) - \frac{1}{L_{\mathrm{Bi}}^2}\widetilde{n}_{\mathrm{Bi}} + \frac{\lambda_{\mathrm{Pb}}}{D_{\mathrm{Bi}}}\widetilde{n}_{\mathrm{Pb}} = 0 \tag{B.23}$$

where we used the definition of the effective ^{212}Bi diffusion length:

$$L_{\mathrm{Bi}} = \sqrt{\frac{D_{\mathrm{Bi}}}{\lambda_{\mathrm{Bi}} + \alpha_{\mathrm{Bi}} - \lambda_{\mathrm{Ra}}}}. \tag{B.24}$$

Following the approach used for ^{212}Pb, we attempt a solution of the form

$$\widetilde{n}_{\mathrm{Bi}}(r) = A_{\mathrm{Bi}}\frac{e^{-r/L_{\mathrm{Rn}}}}{r} + B_{\mathrm{Bi}}\frac{e^{-r/L_{\mathrm{Pb}}}}{r} + C_{\mathrm{Bi}}\frac{e^{-r/L_{\mathrm{Bi}}}}{r}. \tag{B.25}$$

When this solution is substituted into equation (B.23), along with the asymptotic solution for ^{212}Pb, equation (B.16), the terms containing $\frac{e^{-r/L_{\mathrm{Bi}}}}{r}$ cancel out. The coefficients A_{Bi} and B_{Bi} are found by equating the terms containing $\frac{e^{-r/L_{\mathrm{Rn}}}}{r}$ and $\frac{e^{-r/L_{\mathrm{Pb}}}}{r}$, respectively, giving

$$A_{\mathrm{Bi}} = \left(\frac{L_{\mathrm{Rn}}^2 L_{\mathrm{Bi}}^2}{L_{\mathrm{Rn}}^2 - L_{\mathrm{Bi}}^2}\right)\frac{\lambda_{\mathrm{Pb}}}{D_{\mathrm{Bi}}}A_{\mathrm{Pb}} \tag{B.26}$$

$$B_{\mathrm{Bi}} = \left(\frac{L_{\mathrm{Pb}}^2 L_{\mathrm{Bi}}^2}{L_{\mathrm{Pb}}^2 - L_{\mathrm{Bi}}^2}\right)\frac{\lambda_{\mathrm{Pb}}}{D_{\mathrm{Bi}}}B_{\mathrm{Pb}} \tag{B.27}$$

where A_{Pb} and B_{Pb} are given in equation (B.17) and (B.19). Substituting (B.25) into the boundary condition (B.22), gives

$$C_{\mathrm{Bi}} = -\left(A_{\mathrm{Bi}} + B_{\mathrm{Bi}}\right). \tag{B.28}$$

Thus, the asymptotic solution for ^{212}Bi is

$$n_{\mathrm{Bi}}^{asy}(r,t) = \left(A_{\mathrm{Bi}}\frac{e^{-r/L_{\mathrm{Rn}}}}{r} + B_{\mathrm{Bi}}\frac{e^{-r/L_{\mathrm{Pb}}}}{r} + C_{\mathrm{Bi}}\frac{e^{-r/L_{\mathrm{Bi}}}}{r}\right) e^{-\lambda_{\mathrm{Ra}} t} \tag{B.29}$$

where A_{Bi}, B_{Bi} and C_{Bi} are given in equation (B.26), (B.27) and (B.28).

The ratio $L_{\mathrm{Bi}}/L_{\mathrm{Pb}}$ affects the local ratio of ^{212}Bi and ^{212}Pb activities. Figure B1 shows the activity ratio as a function of the radial distance from a point source (in units of L_{Pb}), for varying values of $L_{\mathrm{Bi}}/L_{\mathrm{Pb}}$. The curves do not depend on α_{Bi} and vary only weakly with the ratio $L_{\mathrm{Rn}}/L_{\mathrm{Pb}}$. In order to conform to the experimental data, which shows that the activity ratio is very close to 1.01 (the ratio at secular equilibrium), we must have $L_{\mathrm{Bi}}/L_{\mathrm{Pb}} \lesssim 0.2$ (or less). In terms of the effective diffusion coefficients, this also means that $D_{\mathrm{Bi}}/D_{\mathrm{Pb}} \lesssim 0.3$, assuming that $\alpha_{\mathrm{Bi}} = 0$.

Appendix C. Derivation of the analytic time-dependent solution to the diffusion-leakage model for ^{220}Rn

The time-dependent ^{220}Rn diffusion equation for a point source in an infinite homogeneous and isotropic medium is (for $r > 0$)

$$\frac{\partial n_{\mathrm{Rn}}}{\partial t} = \frac{D_{\mathrm{Rn}}}{r^2}\frac{\partial}{\partial r}\left(r^2\frac{\partial n_{\mathrm{Rn}}}{\partial r}\right) - \lambda_{\mathrm{Rn}} n_{\mathrm{Rn}}. \tag{C.1}$$

With the boundary condition:

$$\lim_{r\to 0} 4\pi r^2 j_{\mathrm{Rn}}^{asy}(r,t) = P_{des}(Rn)\,\Gamma_{\mathrm{Ra}}^{src}(0)\,e^{-\lambda_{\mathrm{Ra}}t} \tag{C.2}$$

and initial condition:

$$n_{\mathrm{Rn}}(r,0) = 0. \tag{C.3}$$

We make the following substitution:

$$n_{\mathrm{Rn}}(r,t) = \frac{e^{-\lambda_{\mathrm{Rn}}t}}{r}\phi(r,t). \tag{C.4}$$

Substituting n_{Rn} in equation (C.1) yields

$$\frac{\partial \phi}{\partial t} = D_{\mathrm{Rn}}\frac{\partial^2 \phi}{\partial r^2}. \tag{C.5}$$

Substituting n_{Rn} in the boundary condition (C.2) gives

$$\phi(0,t) = \frac{P_{des}(Rn)\,\Gamma_{\mathrm{Ra}}^{src}(0)}{4\pi D_{\mathrm{Rn}}} e^{(\lambda_{\mathrm{Rn}}-\lambda_{\mathrm{Ra}})t}. \tag{C.6}$$

From (C.3), the initial condition for ϕ is

$$\phi(r,0) = 0. \tag{C.7}$$

We define the Laplace transform:

$$\Phi(r,s) = \mathcal{L}[\phi(r,t)] = \int_0^\infty \phi(r,t)\,e^{-st}dt. \tag{C.8}$$

We now take the Laplace transform of both sides of equation (C.5). On the left hand side we have:

$$\mathcal{L}\left[\frac{\partial \phi}{\partial t}\right] = s\Phi(r,s) - \phi(r,0) = s\Phi(r,s). \tag{C.9}$$

On the right hand side we have

$$\mathcal{L}\left[D_{\mathrm{Rn}}\frac{\partial^2 \phi}{\partial r^2}\right] = D_{\mathrm{Rn}}\frac{\partial^2 \Phi}{\partial r^2}. \tag{C.10}$$

Thus

$$\frac{\partial^2 \Phi}{\partial r^2} - \frac{s}{D_{\mathrm{Rn}}}\Phi = 0 \tag{C.11}$$

for which the general solution is

$$\Phi = A(s)\,e^{-\sqrt{\frac{s}{D_{\mathrm{Rn}}}}r} + B(s)\,e^{\sqrt{\frac{s}{D_{\mathrm{Rn}}}}r}. \tag{C.12}$$

In order to avoid divergence at $r \to \infty$, we must set $B(s) = 0$ for all s. Hence

$$\Phi(r,s) = A(s)\,e^{-\sqrt{\frac{s}{D_{\mathrm{Rn}}}}r}. \tag{C.13}$$

The coefficient $A(s)$ is found by taking the Laplace transform of the boundary condition (C.6):

$$\begin{aligned}\mathcal{L}[\phi(0,t)] = \Phi(0,s) = A(s) &= \frac{P_{des}(Rn)\,\Gamma_{\mathrm{Ra}}^{src}(0)}{4\pi D_{\mathrm{Rn}}}\mathcal{L}\left[e^{(\lambda_{\mathrm{Rn}}-\lambda_{\mathrm{Ra}})t}\right] \\ &= \frac{P_{des}(Rn)\,\Gamma_{\mathrm{Ra}}^{src}(0)}{4\pi D_{\mathrm{Rn}}}\frac{1}{s-(\lambda_{\mathrm{Rn}}-\lambda_{\mathrm{Ra}})}.\end{aligned} \tag{C.14}$$

Hence

$$\Phi(r,s)=\frac{P_{des}(Rn)\,\Gamma_{\mathrm{Ra}}^{src}(0)}{4\pi D_{\mathrm{Rn}}}\frac{1}{s-(\lambda_{\mathrm{Rn}}-\lambda_{\mathrm{Ra}})}e^{-\sqrt{\frac{s}{D_{\mathrm{Rn}}}}r}. \tag{C.15}$$

We define two auxiliary functions, $F(r,s)$ and $G(s)$:

$$F(r,s)=\frac{P_{des}(Rn)\,\Gamma_{\mathrm{Ra}}^{src}(0)}{4\pi D_{\mathrm{Rn}}}e^{-\sqrt{\frac{s}{D_{\mathrm{Rn}}}}r} \tag{C.16}$$

$$G(s)=\frac{1}{s-(\lambda_{\mathrm{Rn}}-\lambda_{\mathrm{Ra}})} \tag{C.17}$$

so that $\Phi(r,s)=F(r,s)\,G(s)$. We use the identities

$$\mathcal{L}^{-1}\left[\frac{e^{-a\sqrt{s}}}{\pi a}\right]=\frac{1}{2(\pi t)^{3/2}}e^{-\frac{a^2}{4t}} \tag{C.18}$$

$$\mathcal{L}^{-1}\left[\frac{1}{s-a}\right]=e^{at} \tag{C.19}$$

to find the inverse transforms:

$$f(r,t)=\mathcal{L}^{-1}[F(r,s)]=\frac{P_{des}(Rn)\,\Gamma_{\mathrm{Ra}}^{src}(0)\,r}{8(\pi D_{\mathrm{Rn}})^{3/2}}\frac{1}{t^{3/2}}e^{-\frac{r^2}{4D_{\mathrm{Rn}}t}} \tag{C.20}$$

$$g(t)=\mathcal{L}^{-1}[G(s)]=e^{(\lambda_{\mathrm{Rn}}-\lambda_{\mathrm{Ra}})t}. \tag{C.21}$$

We now use the Laplace transform convolution theorem, namely that if $H(s)=\mathcal{L}[h(t)]$ and $H(s)=F(s)\,G(s)$, then $h(t)=\int_0^t f(\tau)\,g(t-\tau)\,d\tau$, where $f(t)=\mathcal{L}^{-1}[F(s)]$ and $g(t)=\mathcal{L}^{-1}[G(s)]$. In our case, $\Phi(s)=F(r,s)\,G(s)$ and hence

$$\begin{aligned}\phi(r,t)&=\mathcal{L}^{-1}[\Phi(r,s)]\\&=\mathcal{L}^{-1}[F(r,s)\,G(s)]\\&=\int_0^t f(r,\tau)\,g(t-\tau)\,d\tau\\&=\frac{P_{des}(Rn)\,\Gamma_{\mathrm{Ra}}^{src}(0)\,r}{8(\pi D_{\mathrm{Rn}})^{3/2}}\int_0^t\frac{1}{\tau^{3/2}}e^{-\frac{r^2}{4D_{\mathrm{Rn}}\tau}}e^{(\lambda_{\mathrm{Rn}}-\lambda_{\mathrm{Ra}})(t-\tau)}d\tau.\end{aligned} \tag{C.22}$$

Finally

$$n_{\mathrm{Rn}}(r,t)=\frac{P_{des}(Rn)\,\Gamma_{\mathrm{Ra}}^{src}(0)\,e^{-\lambda_{\mathrm{Ra}}t}}{8(\pi D_{\mathrm{Rn}})^{3/2}}\int_0^t\frac{1}{\tau^{3/2}}e^{-\frac{r^2}{4D_{\mathrm{Rn}}\tau}}e^{-(\lambda_{\mathrm{Rn}}-\lambda_{\mathrm{Ra}})\tau}d\tau. \tag{C.23}$$

In order to show that this solution converges to the asymptotic form (37), we evaluate the integral in (C.23) in the limit $t\to\infty$. We make the following substitutions: $x^2=\frac{1}{\tau}$, $a=\frac{r^2}{4D_{\mathrm{Rn}}}$ and $b=\lambda_{\mathrm{Rn}}-\lambda_{\mathrm{Ra}}$. The integral now becomes

$$\begin{aligned}&\lim_{t\to\infty}\int_0^t\frac{1}{\tau^{3/2}}e^{-\frac{r^2}{4D_{\mathrm{Rn}}\tau}}e^{-(\lambda_{\mathrm{Rn}}-\lambda_{\mathrm{Ra}})\tau}d\tau=2\int_0^\infty e^{-\left(ax^2+\frac{b}{x^2}\right)}dx\\&=\sqrt{\frac{\pi}{a}}e^{-2\sqrt{ab}}\\&=\frac{2}{r}\sqrt{\pi D_{\mathrm{Rn}}}e^{-2\sqrt{\frac{r^2}{4D_{\mathrm{Rn}}}(\lambda_{\mathrm{Rn}}-\lambda_{\mathrm{Ra}})}}\\&=\frac{2}{r}\sqrt{\pi D_{\mathrm{Rn}}}e^{-r/L_{\mathrm{Rn}}}\end{aligned} \tag{C.24}$$

where use has been made of an integral table to evaluate $\int_0^\infty e^{-\left(ax^2+\frac{b}{x^2}\right)}dx$. Inserting this result into equation (C.23) gives the asymptotic solution (37), as required.

References

Arazi L, Cooks T, Schmidt M, Keisari Y and Kelson I 2007 Treatment of solid tumors by interstitial release of recoiling short-lived alpha emitters *Phys. Med. Biol.* **52** 5025–42

Arazi L, Cooks T, Schmidt M, Keisari Y and Kelson I 2010 The treatment of solid tumors by alpha emitters released from ^{224}Ra-loaded sources-internal dosimetry analysis *Phys. Med. Biol.* **55** 1203

Browne E 2005 Nuclear data sheets for $a = 212$ *Nucl. Data Sheets* **104** 427–96

Cano G L and Dressel R W 1965 Energy loss and resultant charge of recoil particles from alpha disintegrations in surface deposits of ^{210}Po and ^{241}Am *Phys. Rev.* **139** 1883–92

Confino H, Hochman I, Efrati M, Schmidt M, Umansky V, Kelson I and Keisari Y 2015 Tumor ablation by intratumoral Ra-224-loaded wires induces anti-tumor immunity against experimental metastatic tumors *Cancer Immunol. Immunother.* **64** 191–9

Confino H, Schmidt M, Efrati M, Hochman I, Umansky V, Kelson I and Keisari Y 2016 Inhibition of mouse breast adenocarcinoma growth by ablation with intratumoral alpha-irradiation combined with inhibitors of immunosuppression and CPG *Cancer Immunol. Immunother.* **65** 1149–58

Cooks T, Schmidt M, Bittan H, Lazarov E, Arazi L, Kelson I and Keisari Y 2009a Local control of lung derived tumors by diffusing alpha-emitting atoms released from intratumoral wires loaded with radium-224 *Int. J. Radiat. Oncol. Biol. Phys.* **74** 966–73

Cooks T, Arazi L, Efrati M, Schmidt M, Marshak G, Kelson I and Keisari Y 2009b Interstitial wires releasing diffusing alpha emitters combined with chemotherapy improved local tumor control and survival in squamous cell carcinoma-bearing mice *Cancer* **115** 1791–801

Cooks T, Arazi L, Schmidt M, Marshak G, Kelson I and Keisari Y 2008 Growth retardation and destruction of experimental squamous cell carcinoma by interstitial radioactive wires releasing diffusing alpha-emitting atoms *Int. J. Cancer* **122** 1657–64

Cooks T *et al* 2012 Intratumoral ^{224}Ra-loaded wires spread alpha-emitters inside solid human tumors in athymic mice achieving tumor control *Anticancer Res.* **32** 5315–21

Fowler B A 1998 Roles of lead-binding proteins in mediating lead bioavailability *Environ. Health Perspect.* **106** 1585–7

Fowler B A and DuVal G 1991 Effects of lead on the kidney: roles of high-affinity lead-binding proteins *Environ. Health Perspect.* **91** 77–80

Godwin H A 2001 The biological chemistry of lead *Curr. Opin. Chem. Biol.* **5** 223–7

Griffin R M and Matson W R 1972 The assessment of individual variability to trace metal insult: low-molecular-weight metal complexing agents as indicators of trace metal insult *Am. Ind. Hyg. Assoc. J.* **33** 373–7

Gunter K, Asaro F and Helmholz A C 1966 Charge and energy distributions of recoils from ^{226}Th alpha decay *Phys. Rev. Lett.* **16** 362–64

Horev-Drori G, Cooks T, Bittan H, Lazarov E, Schmidt M, Arazi L, Efrati M, Kelson I and Keisari Y 2012 Local control of experimental malignant pancreatic tumors by treatment with a combination of chemotherapy and intratumoral ^{224}radium-loaded wires releasing alpha-emitting atoms *Transl. Res.* **159** 32–41

Jähne B, Heinz G and Dietrich W 1987 Measurement of the diffusion coefficients of sparingly soluble gases in water *J Geophys. Res.* **92** 10767–76

Jain R K 1987 Transport of molecules in the tumor interstitium: a review *Cancer Res.* **47** 3039–51

Jain R K 2001 Delivery of molecular and cellular medicine to solid tumors *Adv. Drug Delivery Rev.* **46** 149–68

Jain R K and Baxter L T 1988 Mechanisms of heterogeneous distribution of monoclonal antibodies and other macromolecules in tumors: significance of elevated interstitial pressure *Cancer Res.* **48** 7022–32

Lazarov E, Arazi L, Efrati M, Cooks T, Schmidt M, Keisari Y and Kelson I 2011 Comparative *in vitro* microdosimetric study of murine- and human-derived cancer cells exposed to alpha particles *Radiat. Res.* **177** 280–7

Leggett R W 1993 An age-specific kinetic model of lead metabolism in humans *Environ. Health Perspect.* **101** 598–616

Lide D R (ed) 2008 *CRC Handbook of Chemistry and Physics* 88th edn (Boca Raton, FL: Taylor and Francis Group)

Martin M J 2007 Nuclear data sheets for $a = 208$ *Nucl. Data Sheets* **108** 1583–806

Milrot E, Jackman A, Flescher E, Gonen P, Kelson I, Keisari Y and Sherman L 2013 Enhanced killing of cervical cancer cells by combinations of methyl jasmonate with cisplatin, x or alpha radiation *Investigational New Drugs* **31** 333–44

NRC 1999 *Risk Assessment of Radon in Drinking Water* (Washington, DC: National Academy Press)

Payne J C, ter Horst M A and Godwin H A 1999 Lead fingers: Pb2 + binding to structural zinc-binding domains determined directly by monitoring lead-thiolate charge-transfer bands *J. Am. Chem. Soc.* **121** 6850–5

Popovtzer A *et al* 2019 Initial safety and tumor control results from a "first-in-human" multicenter prospective trial evaluating a novel alpha-emitting radionuclide for the treatment of locally advanced recurrent squamous cell carcinomas of the skin and head and neck *Int. J. Radiat. Oncol. Biol. Phys.* (accepted) (https://doi.org/10.1016/j.ijrobp.2019.10.048)

Reitkopf-Brodutch S, Confino H, Schmidt M, Cooks T, Efrati M, Arazi L, Rath-Wolfson L, Marshak G, Kelson I and Keisari Y 2015 Ablation of experimental colon cancer by intratumoral 224radium-loaded wires is mediated by alpha particles released from atoms which spread in the tumor and can be augmented by chemotherapy *Int. J. Radiat. Biol.* **91** 179–86

Sgouros G *et al* 2010 Mird pamphlet no. 22 (abridged): radiobiology and dosimetry of alpha-particle emitters for targeted radionuclide therapy *J. Nucl. Med.* **51** 311–28

Smith D, Kahng M, Quintanilla-Vega B and Fowler B 1998 High-affinity renal lead-binding proteins in environmentally-exposed humans *Chem. Biol. Interact.* **115** 39–52

Sonzogni A A 2005 Nudat 2.0: nuclear structure and decay data on the internet *AIP Conf. Proc.* **769** 574–7

Wu S C 2007 Nuclear data sheets for $a = 216$ *Nucl. Data Sheets* **108** 1057–92